



OPEN Mathematical modeling of cholera dynamics in the presence of antimicrobial utilization strategy

Josiah Mushanyu¹✉, Lunga Matsebula² & Farai Nyabadza^{3,4}

Antimicrobial resistance poses a significant threat to public health, particularly in cholera treatment. The emergence of antibiotic resistance, coupled with the sharp decline in pharmaceutical companies developing new cholera antibiotics, is a cause for concern. We formulate a multidrug-resistant (MDR) cholera epidemic model that incorporates a stage-switching strategy between two antibiotics to reduce the magnitude of resistance. The model is analyzed mathematically, and sensitivity analysis of the reproduction number is performed using sub-reproduction numbers. Stability analysis of the cholera-sensitive-only and cholera-resistant-only equilibria is investigated using Centre Manifold Theory. The model is calibrated through Markov Chain Monte Carlo simulations in Stan, showing stability at equilibrium points, which is further verified through numerical simulations. The simulations demonstrate an inverse relationship between the number of MDR cholera cases and the number of individuals receiving second-line treatment for cholera. This study suggests that the correct use of antibiotics can effectively manage the emergence of antimicrobial resistance. From a public health policy perspective, these findings emphasize the importance of antibiotic stewardship programs and the need for policies that promote the responsible use of existing antibiotics while encouraging the development of new treatment options. Such measures could help mitigate the global burden of MDR cholera and prevent further escalation of resistance.

Cholera, a clinical-epidemiologic disease caused by the gram-negative bacterium *Vibrio cholerae*, consists of two pathogenic serogroups: O1 and O139¹. *Vibrio cholerae* O1 has been the predominant strain in recent cholera outbreaks, while *V. cholerae* O139 has declined, now causing only sporadic cases. To date, there have been seven cholera pandemics, collectively responsible for millions of deaths worldwide. The most recent (seventh) pandemic began in South Asia in 1961, spreading to Africa by 1971 and the Americas by 1991². Cholera infection occurs when individuals ingest food or water contaminated with *Vibrio cholerae*³. In its severe form, cholera leads to massive dehydration due to the passage of voluminous “rice-water stools,” which, if left untreated, can result in death in both adults and children³. Cholera remains a significant global public health threat, with Sub-Saharan Africa bearing the majority of the burden (60%) due to inadequate water and sanitation infrastructure⁴. In endemic regions, approximately 1.3 billion people are at risk of cholera, with India, Nigeria, China, Ethiopia, and Bangladesh having the highest at-risk populations⁴. The global burden is estimated at 2.9 million cholera cases annually, resulting in approximately 95,000 deaths⁴. Countries with more than 100,000 cases each year include India, Ethiopia, Nigeria, Haiti, the Democratic Republic of the Congo, Tanzania, Kenya, and Bangladesh⁴. Notably, among the six WHO regions-Africa, the Americas, South-East Asia, Europe, the Eastern Mediterranean, and the Western Pacific-most countries reporting over 1,000 annual cholera deaths are found in the WHO African region⁴. Between 30 June and 31 July 2024, a total of 63,372 new cholera cases and 187 deaths were reported globally⁵. The highest case counts came from Afghanistan (24,951), Yemen (12,825), Pakistan (12,503), Ethiopia (3,491), and Haiti (2,715), while the most deaths were reported in Yemen (47), Ethiopia (46), Nigeria (28), Haiti (22), and Tanzania (11)⁵. Since 1 January 2024, there have been 312,135 cholera cases and 2,284 deaths worldwide⁵. Despite these worrisome statistics, cholera continues to be an overlooked and underreported disease².

Antimicrobial resistance (AMR) is an escalating concern, affecting the treatment of various infections caused by bacteria, viruses, parasites, and fungi. It presents a serious threat to global health and human development⁶. The treatment of infectious diseases in both humans and animals has long relied on antibiotics, making the

¹Department of Computing, Mathematical & Statistical Science, University of Namibia, Windhoek 13301, Namibia.

²Department of Mechanical & Metallurgical Engineering, University of Namibia, Ongwediva 13301, Namibia.

³Department of Mathematics and Applied Mathematics, University of Johannesburg, Johannesburg 2006, South Africa. ⁴Institute of Applied Research and Technology, Dubai International Academic City, Emirates Aviation University, Dubai, UAE. ✉email: mushanyuj@gmail.com

rise of resistance to these critical medicines particularly alarming. Without urgent action, we risk returning to a post-antibiotic era where common infections that were once easily treatable can once again become fatal. AMR pathogens include *Pseudomonas spp.*, *Acinetobacter spp.*, *Klebsiella pneumoniae*, *Streptococcus pneumoniae*, *Salmonella enterica*, *Escherichia coli*, and *Staphylococcus aureus*^{7,8}. The production of new antibiotics has not kept pace with the increasing prevalence of AMR pathogens, especially among Gram-negative bacteria and drug-resistant *Mycobacterium tuberculosis*⁹. Misuse and overuse of antibiotics are major drivers of AMR, as bacterial genomes exhibit high plasticity, allowing for rapid adaptation^{10,11}. Mechanisms of resistance include efflux pumps, genetic mutations, and the transfer of mobile genetic elements such as plasmids and transposons¹², which can be broadly categorized into four types: (i) modification of the antimicrobial compound, (ii) prevention of drug penetration, (iii) target site modification, and (iv) general cellular adaptation mechanisms¹³. The World Health Organization (WHO) recommends tetracycline and ciprofloxacin for the treatment of cholera. Historically, *Vibrio cholerae* has been susceptible to most antibiotics, but resistance has emerged, complicating cholera management. This resistance is often attributed to poor adherence to treatment regimens and indiscriminate antibiotic use^{14,15}. Currently, *Vibrio cholerae* shows resistance to several antibiotics, including tetracycline, ampicillin, streptomycin, and chloramphenicol, due to its adaptive capabilities^{13,16}. Although some strains remain sensitive to ciprofloxacin, others display reduced sensitivity or full resistance, particularly to tetracycline¹². This emphasizes the importance of monitoring cholera strains during outbreaks to detect emerging resistance patterns¹².

Various efforts have been made to model antibiotic resistance. Massad et al.¹⁷ proposed an epidemiological model to examine the spread of antibiotic resistance in bacterial populations. Their model incorporated cross-infection between antibiotic-sensitive and resistant hosts through mutations or plasmid transfer. The results suggested that competitive dynamics between strains are driven by selective pressure from antibiotic treatment. Mushanyu¹⁸ extended the Massad et al. model¹⁷ by developing a four-state system to model community-acquired antibiotic-resistant infections, emphasizing the importance of adherence to proper antibiotic usage. Castillo-Chavez and Feng¹⁹ formulated a two-strain TB transmission model to study the dynamics of resistant TB strains resulting from incomplete antibiotic treatment. Their results confirmed that incomplete treatment often leads to strain coexistence. Webb et al.²⁰ developed a two-tiered population model, incorporating both bacterial and patient levels, to quantify critical factors in nosocomial (hospital-acquired) infections. Their analysis of the dynamics of non-resistant and resistant bacterial strains within hospital epidemic populations offers insights into strategies for preventing the persistence of antibiotic-resistant strains. Haber et al.²¹ developed a stochastic model to examine hospital-acquired infections and resistance, focusing on different strategies for using second-line drugs. Their findings demonstrate that the proposed measures significantly decrease both the incidence of hospital-acquired infections and the occurrence of resistance, with noticeable effects emerging within a few months rather than years. Additionally, they observed that as long as the bacteria remain susceptible to these second-line drugs, switching to them can reduce the overall number of colonized patients and the prevalence of bacteria resistant to these drugs. Chow et al.²² developed a mathematical model to assess the effectiveness of antimicrobial cycling in hospitals, focusing on reducing dual resistance. The model also accounts for physician compliance and the isolation of patients with dual-resistant bacteria. Their findings suggest that while antimicrobials slow the spread of resistance, they alone cannot overcome the issue of drug resistance.

The resistance of *Vibrio cholerae* to antimicrobial agents is a complex challenge, with growing concerns that all commonly used antibiotics may eventually fail due to the bacterium's capacity to evade treatment. This resilience is linked to its ecological adaptability and ability to exchange resistance genes with other bacteria in natural environments and within the human gut microbiome²³. Ongoing genetic surveillance is therefore essential for guiding effective cholera management strategies²⁴. Antimicrobial resistance in cholera also poses a significant threat even to regions considered cholera-free, as proximity to endemic areas and high human mobility heighten the risk of introduction¹². Several modeling efforts have sought to better understand antimicrobial-resistant cholera infection. Mushayabasa and Bhunu²⁵ developed a cholera epidemic model to evaluate the impact of antimicrobial resistance on *Vibrio cholerae* transmission. Their model, which incorporates indirect (environment-to-human) transmission, shows that controlling cholera becomes more difficult if drug-resistant cases outnumber drug-sensitive ones. Safi et al.²⁶ formulated a two-strain cholera model to assess the impact of basic control measures on transmission dynamics, demonstrating that a globally asymptotically stable disease-free equilibrium is achievable when $\mathcal{R}_0 < 1$. These findings suggest that effective cholera control requires a comprehensive strategy combining multiple control measures. Mushanyu et al.²⁷ extended Safi et al.'s model by introducing an antimicrobial resistance cholera epidemic model that incorporates reinfection and integrates interventions such as vaccination, screening, and treatment. Their results emphasize the importance of targeted control strategies in mitigating the spread of antimicrobial-resistant cholera.

Generally, two main approaches are used to model the population biology of drug resistance and treatment: (1) the "population genetics" approach and (2) the "epidemiological" approach²⁸. The first focuses on changes in the frequency of sensitive and resistant bacteria, while the second employs compartmental models to capture infection dynamics. In this paper, we follow the second approach, extending previous cholera models to include both drug-sensitive and drug-resistant strains of *Vibrio cholerae*. Our model captures the transmission dynamics of these two strains and incorporates treatment failure as a driver of drug resistance²⁹. The deterministic compartmental modeling approach has been widely used to study the dynamics of various infectious diseases, including COVID-19^{30,31}, co-infection of malaria and COVID-19³², and co-infection of HIV and Zika virus³³. It has also been applied to model the transmission dynamics of bacterial meningitis³⁴, gonorrhoea³⁵, food-borne diseases³⁶, Ebola³⁷, measles³⁸, and typhoid³⁹. For further insights into the analysis of deterministic compartmental models, readers are referred to discussions by Rahmi et al.⁴⁰, Joshua Kiddy K. Asamoah⁴¹, and Mushanyu et al.⁴². A review on modeling antibiotic resistance⁴³ highlighted the need for pathogen-specific models to better understand resistance mechanisms, multiple colonization phenomena, and transmission risks. In response, we

have developed a novel epidemic model that focuses on the transmission dynamics of *Vibrio cholerae*, specifically exploring the impact of switching from first-line to second-line antibiotics on the incidence and prevalence of cholera. To the best of our knowledge, this is the first model to investigate the spread of multidrug-resistant (MDR) cholera while incorporating antibiotic stage-switching. Unlike existing models that typically assume immediate treatment with effective antibiotics, our model reflects clinical practice, where patients often begin treatment before their antibiotic resistance status is known. This delayed transition between antibiotics adds a layer of realism, particularly in settings where resistance testing is limited. Additionally, the model accounts for both direct (human-to-human) and indirect (environment-to-human) transmission pathways, providing a comprehensive framework for understanding cholera transmission. We hope that this study will stimulate further research in cholera epidemic modeling and contribute to identifying effective strategies for mitigating the global impact of cholera.

The paper is arranged as follows: The next section presents the model formulation and assumptions, while Section “Results” provides an analysis of the equilibrium points and their stability. Numerical simulations are presented in Section “Numerical simulations” to illustrate the theoretical findings, followed by a discussion of the results in Section “Discussion”. Finally, the paper concludes with key recommendations and avenues for future research.

Model formulation

We formulate a pathogen-specific ordinary differential equation model of community-acquired cholera infections that considers a stage-switching of two antibiotics. The human population is designated according to their infection status, with individuals free of *Vibrio cholerae* either belonging to the susceptible class (X) or to the class of recovered (spontaneously or through treatment) individuals (Q). Individuals infected with *Vibrio cholerae* either belong to the untreated class (I) or the class of individuals under treatment (T). The class of untreated infected individuals (I) is subdivided into two classes, namely; untreated infected with strain sensitive to both antibiotics, (I_s), and untreated infected with strain resistant to antibiotic 1, (I_r). We consider cholera treatment via two antibiotic regimens as considered in^{21,44}, that is, (1) *treatment with a standard first-line drug* for which there is some form of resistance and (2) *treatment with second-line drug* for which there is no resistance. Switching to the second-line antibiotic is assumed to happen upon developing resistance to the first-line antibiotic. Thus, individuals under treatment are distinguished according to their treatment status with either the first or second-line antibiotic. The class (T) of individuals under treatment is subdivided into four sub-classes as follows: infected with sensitive strain on treatment with antibiotic 1, (T_{s1}), infected with sensitive strain on treatment with antibiotic 2, (T_{s2}), infected with resistant strain on treatment with antibiotic 1, (T_{r1}) and infected with resistant strain on treatment with antibiotic 2, (T_{r2}). The total human population at any time t is given by

$$N(t) = X(t) + I_s(t) + T_{s1}(t) + T_{s2}(t) + I_r(t) + T_{r1}(t) + T_{r2}(t) + Q(t). \quad (1)$$

We also consider an extra compartment representing the concentration of *Vibrio cholerae* in the environment at any given time t , denoted by $B(t)$. Nelson et al.⁴⁵ discuss bacterial shedding in cholera patients, showing that infected individuals release large amounts of *Vibrio cholerae* into the environment, which significantly contributes to the contamination of water sources. Bacterial contamination of the environment is considered to happen through a natural process at a rate gB enhanced by the excretion of sensitive and resistant bacterial strains from infected individuals in classes I_s and I_r at rates given by ϕ_s and ϕ_r , respectively. The decay process of environmental bacteria is assumed to happen at a rate μ_b . Susceptible individuals are recruited into the population through births or immigration at a rate given by Λ . We consider two transmission pathways for susceptible individuals: primary (environment-to-human) transmission and secondary (human-to-human) transmission. While environment-to-human transmission is the primary mode of cholera spread, the work of Nelson et al.⁴⁵ also emphasizes that direct person-to-person transmission can occur, especially in dense populations where hygiene practices are poor. Susceptible individuals acquire the cholera-sensitive infection either through ingestion of contaminated food and/or water and drinks or through human-to-human transmission at rates $\lambda = \beta \frac{B}{B+k}$ or $\lambda_s = \frac{\beta_s I_s}{N}$ respectively. Here, β represents the transmission rate for humans from the contaminated environment, k is the saturation constant, and β_s represents the human-to-human cholera-sensitive transmission rate. Similarly, susceptible individuals acquire the cholera-resistant infection either through ingestion of contaminated food and/or water and drinks or through human-to-human transmission at rates $\lambda = \beta \frac{B}{B+k}$ or $\lambda_r = \frac{\beta_r I_r}{N}$ respectively. The parameter β_r represents the human-to-human cholera-resistant transmission rate. We assume that once an individual is infected with sensitive or resistant bacteria, they have to be cleared before another bacterial strain can re-colonize them and that there is no superinfection of infected individuals. In this basic model, we consider a period of time such that resistance to the second-line drug has not developed and reinfection has not occurred. We assume that infected individuals are initiated into first-line antibiotic treatment upon first treatment regardless of whether they are colonized with sensitive or resistant bacteria. This means antibiotic 2 is a second-line drug not used upon first treatment. This is considered to capture the realistic situation that, normally, treatment is initiated before the resistance status of an infected individual is known. Thus, untreated infected individuals I_s and I_r may begin treatment with antibiotic 1 at rates respectively given by σ_s and σ_r to join classes T_{s1} and T_{r1} , respectively. Untreated infected individuals I_s and I_r can clear *Vibrio cholerae* spontaneously at rates respectively given by θ_s and θ_r to join the class Q . Similarly, antibiotic-resistant infected individuals treated with first-line antibiotic, T_{r1} , only clear *Vibrio cholerae* spontaneously at rate θ_{r1} to join the Q class, whereas treatment clears *Vibrio cholerae* in T_{s1} individuals

at a rate θ_{s_1} to move into the class Q . Once individuals are in the first-line treatment classes T_{s_1} and T_{r_1} , they are switched to second-line antibiotic at rates σ_{s_1} and σ_{r_1} to join the second-line treatment classes T_{s_2} and T_{r_2} , respectively. Clearance of *Vibrio cholerae* in individuals in classes T_{s_2} and T_{r_2} using second-line antibiotics is assumed to happen at rates θ_{s_2} and θ_{r_2} , to join the class Q . All infected individuals $I_s, T_{s_1}, T_{s_2}, I_r, T_{r_1}, T_{r_2}$ can succumb to cholera infection at rates given by $\delta_s, \delta_{s_1}, \delta_{s_2}, \delta_r, \delta_{r_1}$ and δ_{r_2} , respectively. All individuals experience natural death at a rate given by μ .

Considering the given assumptions, model formulation information, and the schematic diagram above (Fig. 1), we have the following system of equations to model the transmission dynamics of the cholera epidemic in the presence of antibiotic resistance and switching:

$$\left\{ \begin{aligned} \frac{dX}{dt} &= \Lambda - (\mu + \mathcal{A}) X, \\ \frac{dI_s}{dt} &= (f\lambda + \lambda_s) X - (\mu + \delta_s + \theta_s + \sigma_s) I_s, \\ \frac{dT_{s_1}}{dt} &= \sigma_s I_s - (\mu + \delta_{s_1} + \theta_{s_1} + \sigma_{s_1}) T_{s_1}, \\ \frac{dT_{s_2}}{dt} &= \sigma_{s_1} T_{s_1} - (\mu + \delta_{s_2} + \theta_{s_2}) T_{s_2}, \\ \frac{dI_r}{dt} &= ((1-f)\lambda + \lambda_r) X - (\mu + \delta_r + \theta_r + \sigma_r) I_r, \\ \frac{dT_{r_1}}{dt} &= \sigma_r I_r - (\mu + \delta_{r_1} + \theta_{r_1} + \sigma_{r_1}) T_{r_1}, \\ \frac{dT_{r_2}}{dt} &= \sigma_{r_1} T_{r_1} - (\mu + \delta_{r_2} + \theta_{r_2}) T_{r_2}, \\ \frac{dQ}{dt} &= \theta_s I_s + \theta_{s_1} T_{s_1} + \theta_{s_2} T_{s_2} + \theta_r I_r + \theta_{r_1} T_{r_1} + \theta_{r_2} T_{r_2} - \mu Q, \\ \frac{dB}{dt} &= gB + \phi_s I_s + \phi_r I_r - \mu_b B, \end{aligned} \right. \tag{2}$$

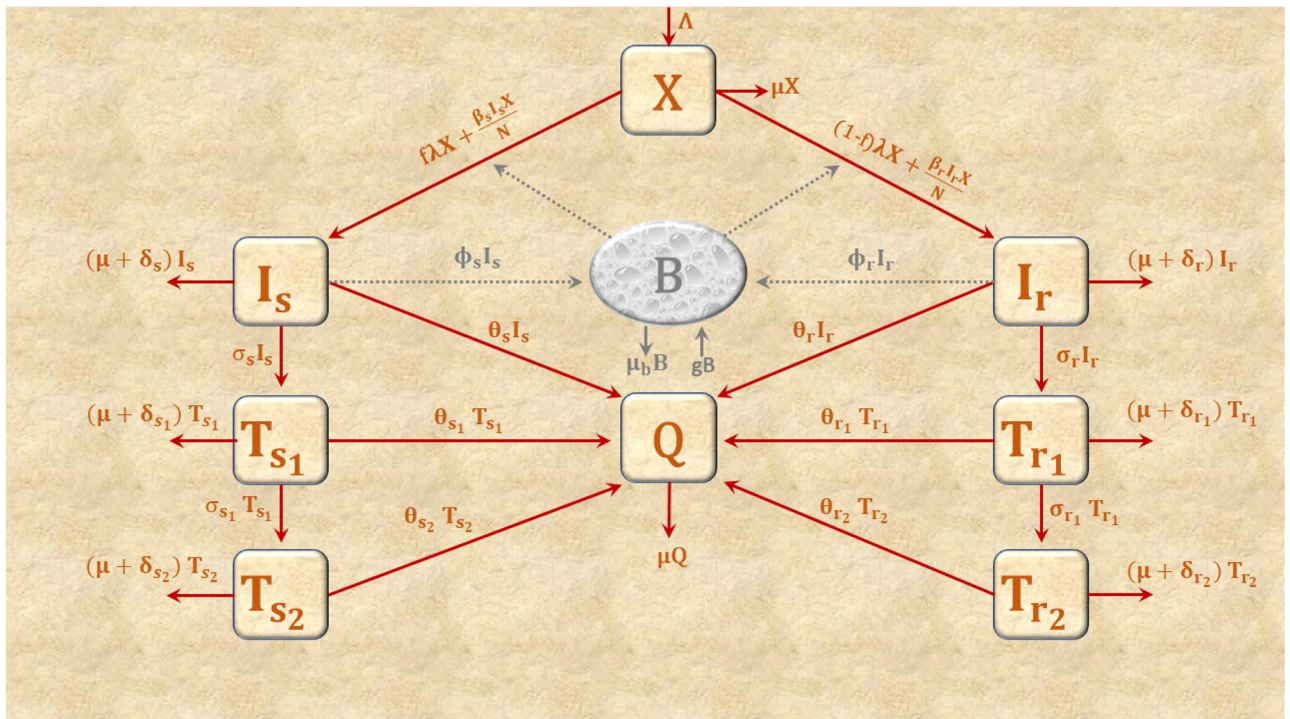


Fig. 1. Model flow diagram.

with initial conditions

$$X(0) > 0, I_s(0) \geq 0, T_{s_1}(0) \geq 0, T_{s_2}(0) \geq 0, I_r(0) \geq 0, T_{r_1}(0) \geq 0, T_{r_2}(0) \geq 0, Q(0) \geq 0, B(0) \geq 0,$$

where $\mathcal{A} = \lambda + \lambda_s + \lambda_r$, we assume that all the model parameters are non-negative.

Results

In this section, we shall perform some theoretical analysis of the model to illustrate that it is biologically meaningful.

Positivity of solutions

In biological and epidemiological models, state variables often represent quantities that cannot be negative, such as population sizes. Since the model tracks both the human population and bacteria population, it is necessary to establish that the model solutions remain non-negative for any given future time t regardless of the choice of initial conditions. Ensuring positivity is crucial for the validity and applicability of the model. We state the following theorem.

Theorem 1

$$X(0) > 0, I_s(0) \geq 0, T_{s_1}(0) \geq 0, T_{s_2}(0) \geq 0, I_r(0) \geq 0, T_{r_1}(0) \geq 0, T_{r_2}(0) \geq 0, Q(0) \geq 0, B(0) \geq 0,$$

be the given initial conditions of system (2). Then, there exists $(X(t), I_s(t), T_{s_1}(t), T_{s_2}(t), I_r(t), T_{r_1}(t), T_{r_2}(t), Q(t), B(t)) \in \mathbb{R}_+^9$ which solve system (2).

Proof Let $\hat{t} \in [0, t]$ be the maximum time value satisfying

$$\hat{t} = \sup \{t > 0 : X > 0, I_s > 0, T_{s_1} > 0, T_{s_2} > 0, I_r > 0, T_{r_1} > 0, T_{r_2} > 0, Q > 0, B > 0\} \in [0, t].$$

Thus, it follows from the first equation of system (2) that

$$\frac{dX}{dt} = \Lambda - (\mu + \lambda + \lambda_s + \lambda_r) X \geq \Lambda - (\mu + \lambda + \Delta_s + \Delta_r) X$$

where $\Delta_s = \beta_s I_s$ and $\Delta_r = \beta_r I_r$ with $\lambda = \beta \frac{B}{B+k}$, $\lambda_s = \frac{\beta_s I_s}{N}$ and $\lambda_r = \frac{\beta_r I_r}{N}$. The above differential inequality can be easily solved using the integrating factor technique. Making use of the convenient definition

$$\mathcal{A} = \lambda + \Delta_s + \Delta_r$$

we obtain

$$\begin{aligned} \frac{d}{dt} \left[X(t) \exp \left(\mu t + \int_0^t \mathcal{A}(s) ds \right) \right] &\geq \Lambda \exp \left(\mu t + \int_0^t \mathcal{A}(s) ds \right), \\ \Rightarrow X(\hat{t}) &\geq X(0) \exp \left[- \left(\mu \hat{t} + \int_0^{\hat{t}} \mathcal{A}(s) ds \right) \right] \\ &+ \exp \left[- \left(\mu \hat{t} + \int_0^{\hat{t}} \mathcal{A}(s) ds \right) \right] \times \left[\int_0^{\hat{t}} \Lambda \exp \left(\mu \hat{t} + \int_0^{\hat{t}} \mathcal{A}(\nu) d\nu \right) d\hat{t} \right] > 0. \end{aligned}$$

Thus, the susceptible population, X , will remain non-negative for any time t regardless of the given initial condition $X(0) > 0$. We now consider the class of individuals infected by the sensitive strain I_s . We make use of the second equation of system (2) to obtain

$$\begin{aligned} \frac{dI_s}{dt} &= (f\lambda + \lambda_s) X - (\mu + \delta_s + \theta_s + \sigma_s) I_s \geq -(\mu + \delta_s + \theta_s + \sigma_s) I_s, \\ \Rightarrow I_s(\hat{t}) &\geq I_s(0) \exp \left[-(\mu + \delta_s + \theta_s + \sigma_s) \hat{t} \right] > 0. \end{aligned}$$

Thus, the class I_s of individuals infected by the sensitive strain will remain non-negative for any time t regardless of the given initial condition $I_s(0) > 0$. Following the outlined computations, similar results can also be obtained for the remaining classes. This completes the proof. \square

The set of biological interest is given as follows:

$$\Omega = \left\{ (X(t), I_s(t), T_{s1}(t), T_{s2}(t), I_r(t), T_{r1}(t), T_{r2}(t), Q(t), B(t)) \in \mathbb{R}_+^9, N \leq \frac{\Lambda}{\mu}, B \leq \frac{(\phi_s + \phi_r)\Lambda}{\mu(\mu_b - g)} \right\}. \quad (3)$$

We now state the following lemma that guarantees system (2) makes biological sense, that is, all solutions starting in (3) will remain there for all time t .

Lemma 1 *The compact set Ω defined in (3) is positively invariant for the solutions of system (2) in \mathbb{R}_+^9 .*

Proof Considering the equations for human compartments in system (2), we obtain

$$\frac{dN}{dt} = \Lambda - \mu N - \delta_s I_s - \delta_{s1} I_{s1} - \delta_{s2} I_{s2} - \delta_r I_r - \delta_{r1} I_{r1} - \delta_{r2} I_{r2} \leq \Lambda - \mu N.$$

Define $\mathcal{P}(t) = (N(t), B(t)) = (X(t) + I_s(t) + T_{s1}(t) + T_{s2}(t) + I_r(t) + T_{r1}(t) + T_{r2}(t) + Q(t), B(t))$. The time derivative of $\mathcal{P}(t)$ is obtained as follows

$$\begin{aligned} \frac{d\mathcal{P}}{dt} &= \left(\frac{dN}{dt}, \frac{dB}{dt} \right) = \left(\frac{dX}{dt} + \frac{dI_s}{dt} + \frac{dT_{s1}}{dt} + \frac{dT_{s2}}{dt} + \frac{dI_r}{dt} + \frac{dT_{r1}}{dt} + \frac{dT_{r2}}{dt} + \frac{dQ}{dt}, \frac{dB}{dt} \right) \\ &= (\Lambda - \mu N - \delta_s I_s - \delta_{s1} I_{s1} - \delta_{s2} I_{s2} - \delta_r I_r - \delta_{r1} I_{r1} - \delta_{r2} I_{r2}, (g - \mu_b) B + \phi_s I_s + \phi_r I_r). \end{aligned}$$

The time derivative of $N(t)$ simplifies to

$$\frac{dN}{dt} = \Lambda - \mu N - \delta_s I_s - \delta_{s1} I_{s1} - \delta_{s2} I_{s2} - \delta_r I_r - \delta_{r1} I_{r1} - \delta_{r2} I_{r2} \leq \Lambda - \mu N \leq 0, \quad \text{for } N \geq \frac{\Lambda}{\mu}. \quad (4)$$

Also, the time derivative of $B(t)$ simplifies to

$$\begin{aligned} \frac{dB}{dt} &= (g - \mu_b) B + \phi_s I_s + \phi_r I_r \leq (g - \mu_b) B + (\phi_s + \phi_r) N \leq 0, \quad \text{for} \\ B &\geq \frac{(\phi_s + \phi_r)\Lambda}{\mu(\mu_b - g)} \quad \text{with } N \geq \frac{\Lambda}{\mu} \text{ and } \mu_b > g. \end{aligned} \quad (5)$$

Combining results from (4) and (5), we have that $\frac{d\mathcal{P}}{dt} \leq 0$ which implies that Ω is a positively invariant set. Further, solving (4) gives

$$0 \leq N(t) \leq \frac{\Lambda}{\mu} + N(0)e^{-\mu t}. \quad (6)$$

Also, solving (5) gives

$$0 \leq B(t) \leq \frac{(\phi_s + \phi_r)\Lambda}{\mu(\mu_b - g)} + B(0)e^{-(g - \mu_b)t}. \quad (7)$$

Taking time limits in both (6) and (7) gives

$$0 \leq (N(t), B(t)) \leq \left(\frac{\Lambda}{\mu}, \frac{(\phi_s + \phi_r)\Lambda}{\mu(\mu_b - g)} \right) \quad \text{as } t \rightarrow \infty.$$

Hence, Ω is an attractive set. This completes the proof. □

Cholera-free equilibrium and the reproduction number

In this section, we establish the existence of an infection-free equilibrium where neither the sensitive strain nor the resistant strain is present in the population. We set all the infection compartments to zero, that is,

$$I_s = T_{s1} = T_{s2} = I_r = T_{r1} = T_{r2} = Q = B = 0.$$

Thus, before infection, the system is at the cholera-free equilibrium given by

$$\mathcal{E}_0 = \left(\frac{\Lambda}{\mu}, 0, 0, 0, 0, 0, 0, 0, 0 \right). \quad (8)$$

Once the *Vibrio cholerae* bacteria invade the population, the cholera infection can spread in the community. To measure the potential for cholera progression in the presence of antibiotic treatment, we compute a quantity called the reproduction number, denoted by \mathcal{R}_c . This entails the average number of new cholera infections each cholera-infected individual generates in a fully susceptible population. The reproduction number is a key metric in public health, serving as a fundamental tool for guiding interventions and managing epidemics. It helps evaluate the effectiveness of control measures and informs the development of strategies to reduce the spread of infectious diseases. The reproduction number is computed using the next-generation matrix approach outlined in detail in van den Driessche and Watmough⁴⁶. Following this approach, we have

$$F = \begin{pmatrix} \beta_s & 0 & 0 & 0 & 0 & 0 & \frac{\beta f \Lambda}{k\mu} \\ 0 & 0 & 0 & 0 & 0 & 0 & 0 \\ 0 & 0 & 0 & 0 & 0 & 0 & 0 \\ 0 & 0 & 0 & \beta_r & 0 & 0 & \frac{\beta(1-f)\Lambda}{k\mu} \\ 0 & 0 & 0 & 0 & 0 & 0 & 0 \\ 0 & 0 & 0 & 0 & 0 & 0 & 0 \\ 0 & 0 & 0 & 0 & 0 & 0 & 0 \end{pmatrix} \quad \text{and} \quad V = \begin{pmatrix} h_s & 0 & 0 & 0 & 0 & 0 & 0 \\ -\sigma_s & h_{s1} & 0 & 0 & 0 & 0 & 0 \\ 0 & -\sigma_{s1} & h_{s2} & 0 & 0 & 0 & 0 \\ 0 & 0 & 0 & h_r & 0 & 0 & 0 \\ 0 & 0 & 0 & -\sigma_r & h_{r1} & 0 & 0 \\ 0 & 0 & 0 & 0 & -\sigma_{r1} & h_{r2} & 0 \\ -\phi_s & 0 & 0 & -\phi_r & 0 & 0 & \mu_b - g \end{pmatrix}.$$

This leads to

$$F \cdot V^{-1} = \begin{pmatrix} f\mathcal{R}_{\mathcal{B}_s} + \mathcal{R}_{\mathcal{H}_s} & 0 & 0 & f\mathcal{R}_{\mathcal{B}_r} & 0 & 0 & f\mathcal{R}_B \\ 0 & 0 & 0 & 0 & 0 & 0 & 0 \\ 0 & 0 & 0 & 0 & 0 & 0 & 0 \\ (1-f)\mathcal{R}_{\mathcal{B}_s} & 0 & 0 & (1-f)\mathcal{R}_{\mathcal{B}_r} + \mathcal{R}_{\mathcal{H}_r} & 0 & 0 & (1-f)\mathcal{R}_B \\ 0 & 0 & 0 & 0 & 0 & 0 & 0 \\ 0 & 0 & 0 & 0 & 0 & 0 & 0 \\ 0 & 0 & 0 & 0 & 0 & 0 & 0 \end{pmatrix},$$

where

$$\mathcal{R}_{\mathcal{B}_s} = \frac{\beta\Lambda\phi_s}{k\mu h_s(\mu_b - g)}, \quad \mathcal{R}_{\mathcal{H}_s} = \frac{\beta_s}{h_s}, \quad \mathcal{R}_{\mathcal{B}_r} = \frac{\beta\Lambda\phi_r}{k\mu h_r(\mu_b - g)}, \quad \mathcal{R}_{\mathcal{H}_r} = \frac{\beta_r}{h_r}, \quad \mathcal{R}_B = \frac{\beta\Lambda}{k\mu(\mu_b - g)},$$

$$h_s = \mu + \delta_s + \theta_s + \sigma_s, \quad h_{s1} = \mu + \delta_{s1} + \theta_{s1} + \sigma_{s1}, \quad h_{s2} = \mu + \delta_{s2} + \theta_{s2},$$

$$h_r = \mu + \delta_r + \theta_r + \sigma_r, \quad h_{r1} = \mu + \delta_{r1} + \theta_{r1} + \sigma_{r1}, \quad h_{r2} = \mu + \delta_{r2} + \theta_{r2}.$$

Thus, the reproduction number is given by

$$\mathcal{R}_c = \frac{1}{2} \left[(1-f)\mathcal{R}_{\mathcal{B}_r} + \mathcal{R}_{\mathcal{H}_r} + f\mathcal{R}_{\mathcal{B}_s} + \mathcal{R}_{\mathcal{H}_s} + \sqrt{((1-f)\mathcal{R}_{\mathcal{B}_r} + \mathcal{R}_{\mathcal{H}_r} + f\mathcal{R}_{\mathcal{B}_s} + \mathcal{R}_{\mathcal{H}_s})^2 - 4((1-f)\mathcal{R}_{\mathcal{B}_r}\mathcal{R}_{\mathcal{H}_s} + f\mathcal{R}_{\mathcal{B}_s}\mathcal{R}_{\mathcal{H}_r} + \mathcal{R}_{\mathcal{H}_r}\mathcal{R}_{\mathcal{H}_s})} \right]. \tag{9}$$

The reproduction number \mathcal{R}_c is biologically feasible provided

$$((1-f)\mathcal{R}_{\mathcal{B}_r} + \mathcal{R}_{\mathcal{H}_r} + f\mathcal{R}_{\mathcal{B}_s} + \mathcal{R}_{\mathcal{H}_s})^2 \geq 4((1-f)\mathcal{R}_{\mathcal{B}_r}\mathcal{R}_{\mathcal{H}_s} + f\mathcal{R}_{\mathcal{B}_s}\mathcal{R}_{\mathcal{H}_r} + \mathcal{R}_{\mathcal{H}_r}\mathcal{R}_{\mathcal{H}_s}) \quad \text{and} \quad \mu_b > g. \tag{10}$$

Take note that the reproduction number \mathcal{R}_c is a combination of four sub-reproduction numbers $\mathcal{R}_{\mathcal{B}_s}$, $\mathcal{R}_{\mathcal{H}_s}$, $\mathcal{R}_{\mathcal{B}_r}$ and $\mathcal{R}_{\mathcal{H}_r}$ defined as follows.

Sub-reproduction number 1 The sub-reproduction number, $\mathcal{R}_{\mathcal{B}_s} = \frac{\beta\Lambda\phi_s}{k\mu h_s(\mu_b - g)}$, represents the contribution of sensitive bacteria in the environment.

Sub-reproduction number 2 The sub-reproduction number, $\mathcal{R}_{\mathcal{H}_s} = \frac{\beta_s}{h_s}$, represents the contribution of individuals infected by the sensitive strain, I_s .

Sub-reproduction number 3 The sub-reproduction number, $\mathcal{R}_{\mathcal{B}_r} = \frac{\beta\Lambda\phi_r}{k\mu h_r(\mu_b - g)}$, represents the contribution of resistant bacteria in the environment.

Sub-reproduction number 4 The sub-reproduction number, $\mathcal{R}_{\mathcal{H}_r} = \frac{\beta_r}{h_r}$, represents the contribution of individuals infected by the resistant strain, I_r .

Since the model considers the existence of two strains of cholera infections, it means that infected individuals harbor either of these strains. Thus, the expectation is that an individual infected with a sensitive strain will only be capable of transmitting the sensitive strain to susceptible individuals, and resistant strain-infected individuals

will only be capable of transmitting the resistant strain to susceptible individuals. This feature should be reflected in the terms of the reproduction number. We consider the following two possible cases:

Case 1 In the absence of the resistance strain, we have that $\mathcal{R}_{\mathcal{B}_r} = \mathcal{R}_{\mathcal{H}_r} = 0$ and $f = 1$. Thus, for this case, we obtain the sensitive-only reproduction number given by

$$\mathcal{R}_{cs} = \frac{1}{2} \left[f\mathcal{R}_{\mathcal{B}_s} + \mathcal{R}_{\mathcal{H}_s} + \sqrt{(f\mathcal{R}_{\mathcal{B}_s} + \mathcal{R}_{\mathcal{H}_s})^2} \right] = f\mathcal{R}_{\mathcal{B}_s} + \mathcal{R}_{\mathcal{H}_s} = \mathcal{R}_{\mathcal{B}_s} + \mathcal{R}_{\mathcal{H}_s}. \tag{11}$$

Case 2 In the absence of the sensitive strain, we have that $\mathcal{R}_{\mathcal{B}_s} = \mathcal{R}_{\mathcal{H}_s} = 0$ and $f = 0$. Thus, for this case, we obtain the resistance-only reproduction number given by

$$\mathcal{R}_{cr} = \frac{1}{2} \left[(1-f)\mathcal{R}_{\mathcal{B}_r} + \mathcal{R}_{\mathcal{H}_r} + \sqrt{((1-f)\mathcal{R}_{\mathcal{B}_r} + \mathcal{R}_{\mathcal{H}_r})^2} \right] = (1-f)\mathcal{R}_{\mathcal{B}_r} + \mathcal{R}_{\mathcal{H}_r} = \mathcal{R}_{\mathcal{B}_r} + \mathcal{R}_{\mathcal{H}_r}. \tag{12}$$

Local stability of the cholera-free steady state

We show the local stability of the cholera-free equilibrium point \mathcal{C}_0 . The local stability of the cholera-free equilibrium point \mathcal{C}_0 implies that cholera can be eradicated from the population if the initial sizes of the model compartments are within its basin of attraction. Specifically, under the conditions $\mathcal{R}_{\mathcal{H}_s} < 1$, $\mathcal{R}_{\mathcal{H}_r} < 1$, and $\frac{(1-f)\mathcal{R}_{\mathcal{B}_r}}{\mathcal{R}_{\mathcal{H}_r}-1} + \frac{f\mathcal{R}_{\mathcal{B}_s}}{\mathcal{R}_{\mathcal{H}_s}-1} < 1$, cholera transmission will die out. These conditions highlight the importance of controlling both human-to-human and environment-to-human transmission for successful disease eradication.

Theorem 2 The cholera-free equilibrium point \mathcal{C}_0 of system (2) is locally asymptotically stable if $\mathcal{R}_{\mathcal{H}_s} < 1$, $\mathcal{R}_{\mathcal{H}_r} < 1$ and $\frac{(1-f)\mathcal{R}_{\mathcal{B}_r}}{\mathcal{R}_{\mathcal{H}_r}-1} + \frac{f\mathcal{R}_{\mathcal{B}_s}}{\mathcal{R}_{\mathcal{H}_s}-1} < 1$ and is unstable if $\mathcal{R}_{\mathcal{H}_s} > 1$ or $\mathcal{R}_{\mathcal{H}_r} > 1$ or $\frac{(1-f)\mathcal{R}_{\mathcal{B}_r}}{\mathcal{R}_{\mathcal{H}_r}-1} + \frac{f\mathcal{R}_{\mathcal{B}_s}}{\mathcal{R}_{\mathcal{H}_s}-1} > 1$.

Proof We evaluate the Jacobian matrix for system (2) at \mathcal{C}_0 to obtain

$$J(\mathcal{C}_0) = \begin{pmatrix} -\mu & -\beta_s & 0 & 0 & -\beta_r & 0 & 0 & -\frac{\beta\Lambda}{k\mu} \\ 0 & \beta_s - h_s & 0 & 0 & 0 & 0 & 0 & \frac{\beta f\Lambda}{k\mu} \\ 0 & \sigma_s & -h_{s1} & 0 & 0 & 0 & 0 & 0 \\ 0 & 0 & \sigma_{s1} & -h_{s2} & 0 & 0 & 0 & 0 \\ 0 & 0 & 0 & 0 & \beta_r - h_r & 0 & 0 & \frac{\beta(1-f)\Lambda}{k\mu} \\ 0 & 0 & 0 & 0 & \sigma_r & -h_{r1} & 0 & 0 \\ 0 & 0 & 0 & 0 & 0 & \sigma_{r1} & -h_{r2} & 0 \\ 0 & \phi_s & 0 & 0 & \phi_r & 0 & 0 & g - \mu_b \end{pmatrix}.$$

It can be noted that $-\mu$ is an eigenvalue of $J(\mathcal{C}_0)$. Thus, the local stability of \mathcal{C}_0 can be determined by the following submatrix of $J(\mathcal{C}_0)$,

$$\bar{J}(\mathcal{C}_0) = \begin{pmatrix} \beta_s - h_s & 0 & 0 & 0 & 0 & 0 & \frac{\beta f\Lambda}{k\mu} \\ \sigma_s & -h_{s1} & 0 & 0 & 0 & 0 & 0 \\ 0 & \sigma_{s1} & -h_{s2} & 0 & 0 & 0 & 0 \\ 0 & 0 & 0 & \beta_r - h_r & 0 & 0 & \frac{\beta(1-f)\Lambda}{k\mu} \\ 0 & 0 & 0 & \sigma_r & -h_{r1} & 0 & 0 \\ 0 & 0 & 0 & 0 & \sigma_{r1} & -h_{r2} & 0 \\ \phi_s & 0 & 0 & \phi_r & 0 & 0 & g - \mu_b \end{pmatrix}.$$

Note that the off-diagonal entries of $\bar{J}(\mathcal{C}_0)$ are all positive. We claim that $-\bar{J}(\mathcal{C}_0)$ is an M -matrix. Consider the 7×1 matrix

$$Y_1 = [y_1, y_2, y_3, y_4, y_5, y_6, y_7]^T$$

where

$$\begin{cases} y_1 = \frac{y_6 h_{r1} h_{r2} (k\mu (\mu_b - g) (h_r - \beta_r) - \beta(1 - f)\Lambda\phi_r)}{\beta(1 - f)\Lambda\sigma_r\sigma_{r1}\phi_s}, \\ y_2 = \frac{y_6 h_{r1} h_{r2} \sigma_s (k\mu (\mu_b - g) (h_r - \beta_r) - \beta(1 - f)\Lambda\phi_r)}{\beta(1 - f)\Lambda h_{s1} \sigma_r \sigma_{r1} \phi_s}, \\ y_3 = \frac{y_6 h_{r1} h_{r2} \sigma_s \sigma_{s1} (k\mu (\mu_b - g) (h_r - \beta_r) - \beta(1 - f)\Lambda\phi_r)}{\beta(1 - f)\Lambda h_{s1} h_{s2} \sigma_r \sigma_{r1} \phi_s}, \\ y_4 = \frac{y_6 h_{r1} h_{r2}}{\sigma_r \sigma_{r1}}, \quad y_5 = \frac{y_6 h_{r2}}{\sigma_{r1}}, \quad y_6 = y_6 > 0, \quad y_7 = \frac{k\mu y_6 h_{r1} h_{r2} (h_r - \beta_r)}{\beta(1 - f)\Lambda\sigma_r\sigma_{r1}}. \end{cases} \tag{13}$$

Multiplying matrix $-\bar{J}(\mathcal{C}_0)$ by Y_1 gives

$$-\bar{J}(\mathcal{C}_0) \cdot Y_1 = \left[1 - \left(\frac{(1-f)\mathcal{R}_{\mathcal{B}r}}{\mathcal{R}_{\mathcal{H}r} - 1} + \frac{f\mathcal{R}_{\mathcal{B}s}}{\mathcal{R}_{\mathcal{H}s} - 1} \right) \right] \cdot Y_2$$

where Y_2 is a positive 7×1 matrix given by $Y_2 = [P, 0, 0, 0, 0, 0, 0]^T$. Here, P is defined as

$$P = \frac{k\mu h_{r1} h_{r2} y_6 (\mu_b - g) (\mathcal{R}_{\mathcal{H}s} - 1) (\mathcal{R}_{\mathcal{H}r} - 1)}{(1 - f)\beta\Lambda\sigma_r\sigma_{r1}\phi_s} \tag{14}$$

which is positive for $\mathcal{R}_{\mathcal{H}s} < 1$ and $\mathcal{R}_{\mathcal{H}r} < 1$. Thus, since $-\bar{J}(\mathcal{C}_0)$ is an M -matrix, it follows that all the eigenvalues of $\bar{J}(\mathcal{C}_0)$ have negative real parts only if $\frac{(1-f)\mathcal{R}_{\mathcal{B}r}}{\mathcal{R}_{\mathcal{H}r} - 1} + \frac{f\mathcal{R}_{\mathcal{B}s}}{\mathcal{R}_{\mathcal{H}s} - 1} < 1$. Therefore, the cholera-free equilibrium point \mathcal{C}_0 is locally asymptotically stable provided all the stated conditions below hold:

$$\mathcal{R}_{\mathcal{H}s} < 1, \quad \mathcal{R}_{\mathcal{H}r} < 1 \quad \text{and} \quad \frac{(1-f)\mathcal{R}_{\mathcal{B}r}}{\mathcal{R}_{\mathcal{H}r} - 1} + \frac{f\mathcal{R}_{\mathcal{B}s}}{\mathcal{R}_{\mathcal{H}s} - 1} < 1.$$

On the other hand, it can be established that the determinant of $\bar{J}(\mathcal{C}_0)$ is given by

$$\det \bar{J}(\mathcal{C}_0) = \left[\left(\frac{(1-f)\mathcal{R}_{\mathcal{B}r}}{\mathcal{R}_{\mathcal{H}r} - 1} + \frac{f\mathcal{R}_{\mathcal{B}s}}{\mathcal{R}_{\mathcal{H}s} - 1} \right) - 1 \right] P.$$

Thus, if $\frac{(1-f)\mathcal{R}_{\mathcal{B}r}}{\mathcal{R}_{\mathcal{H}r} - 1} + \frac{f\mathcal{R}_{\mathcal{B}s}}{\mathcal{R}_{\mathcal{H}s} - 1} < 1$ with $\mathcal{R}_{\mathcal{H}s} < 1$ and $\mathcal{R}_{\mathcal{H}r} < 1$, then the matrix $\bar{J}(\mathcal{C}_0)$ has eigenvalues with negative real parts, which implies stability of \mathcal{C}_0 . This completes the proof. \square

Sensitivity analysis

We now perform the sensitivity analysis on the reproduction and sub-reproduction numbers. Sensitivity analysis helps to assess which model parameters have the greatest impact on the value of the reproduction number. Sensitivity indices indicate how sensitive the reproduction number is to a change in each parameter. In other words, identifying such parameters is crucial in the control of both sensitive and resistant cholera infection. The sensitivity indices are computed following Chitnis et al.⁴⁷. There are usually errors in data collection and uncertainty in presumed parameter values. Thus, sensitivity analysis is useful in determining the robustness of model predictions to parameter values Chitnis et al.⁴⁷. The normalized forward sensitivity index (NFSI) of the reproduction number is the relative change in the variable reproduction number to the relative change in a given parameter. A positive sensitivity index entails increasing/decreasing the parameter value, which increases/decreases the value of the reproduction number. In that case, we say that the sensitivity index is directly proportional. A negative sensitivity index entails increasing the parameter value, which results in a decrease in the value of the reproduction number. In that case, we say that the sensitivity index is inversely proportional. It is unethical to compute the sensitivity of the parameters $\mu, \delta_s, \delta_{s1}, \delta_{s2}, \delta_r, \delta_{r1}$ and δ_{r2} as these involve the natural and disease-related deaths of humans. Recalling that $\mu_b > g$, we compute the sensitivity indices of the reproduction numbers below.

Sensitivity analysis of the sub-reproduction numbers

Sensitivity analysis of sub-reproduction number 1 We perform sensitivity analysis on the sub-reproduction number $\mathcal{R}_{\mathcal{B}s} = \frac{\beta\Lambda\phi_s}{k\mu h_s (\mu_b - g)}$. It can be observed that parameters β, Λ , and ϕ_s have directly proportional sensitivity indices while parameters k, θ_s , and σ_s have inversely proportional sensitivity indices. The sensitivity indices of μ_b and g are computed as follows:

$$\frac{\partial \mathcal{R}_{\mathcal{B}s}}{\partial \mu_b} \times \frac{\mu_b}{\mathcal{R}_{\mathcal{B}s}} = -\frac{\mu_b}{\mu_b - g} < 0 \quad \text{and} \quad \frac{\partial \mathcal{R}_{\mathcal{B}s}}{\partial g} \times \frac{g}{\mathcal{R}_{\mathcal{B}s}} = \frac{g}{\mu_b - g} > 0. \tag{15}$$

Thus, the parameter g has a directly proportional sensitivity index while the parameter μ_b has an inversely proportional sensitivity index.

Sensitivity analysis of sub-reproduction number 2 We perform sensitivity analysis on the sub-reproduction number $\mathcal{R}_{\mathcal{H}_s} = \frac{\beta_s}{h_s}$. It can be observed that the parameter β_s has a directly proportional sensitivity index while parameters θ_s and σ_s have inversely proportional sensitivity indices.

Sensitivity analysis of sub-reproduction number 3 We perform sensitivity analysis on the sub-reproduction number $\mathcal{R}_{\mathcal{B}_r} = \frac{\beta\Lambda\phi_r}{k\mu h_r(\mu_b - g)}$. It can be clearly observed that parameters g, β, Λ and ϕ_s have directly proportional sensitivity indices while parameters μ_b, k, θ_s and σ_s have inversely proportional sensitivity indices.

Sensitivity analysis of sub-reproduction number 4 We perform sensitivity analysis on the sub-reproduction number $\mathcal{R}_{\mathcal{H}_r} = \frac{\beta_r}{h_r}$. It can be observed that the parameter β_r has a directly proportional sensitivity index while parameters θ_r and σ_r have inversely proportional sensitivity indices.

Since the reproduction number \mathcal{R}_c is a combination of four sub-reproduction numbers $\mathcal{R}_{\mathcal{B}_s}, \mathcal{R}_{\mathcal{H}_s}, \mathcal{R}_{\mathcal{B}_r}$ and $\mathcal{R}_{\mathcal{H}_r}$, the sensitivity analysis results for the reproduction number \mathcal{R}_c can be inferred from the sensitivity analysis results of the sub-reproduction numbers.

Cholera-persistent equilibrium points

In this section, we compute the possible cholera-persistent equilibrium points for system (2). We observe that for system (2), there are three possible endemic equilibria, namely: (1) cholera-sensitive only equilibrium, (2) cholera-resistant only equilibrium, and (3) the interior endemic equilibrium where both cholera strains exist.

Cholera-sensitive only equilibrium

In this section, we compute the cholera-sensitive only equilibrium, denoted by, $\mathcal{C}^\circ = (X^\circ, I_s^\circ, T_{s1}^\circ, T_{s2}^\circ, B^\circ)$. This is obtained by setting $I_r = T_{r1} = T_{r2} = 0$ in system (2) and solving the following system of equations

$$\begin{cases} 0 = \Lambda - \mu X^\circ - \left(\frac{\beta B^\circ}{B^\circ + k} + \frac{\beta_s I_s^\circ}{X^\circ + I_s^\circ + T_{s1}^\circ + T_{s2}^\circ} \right) X^\circ, \\ 0 = \left(\frac{\beta B^\circ}{B^\circ + k} + \frac{\beta_s I_s^\circ}{X^\circ + I_s^\circ + T_{s1}^\circ + T_{s2}^\circ} \right) X^\circ - h_s I_s^\circ, \\ 0 = \sigma_s I_s^\circ - h_{s1} T_{s1}^\circ, \\ 0 = \sigma_{s1} T_{s1}^\circ - h_{s2} T_{s2}^\circ, \\ 0 = g B^\circ + \phi_s I_s^\circ - \mu_b B^\circ. \end{cases} \tag{16}$$

From the third, fourth, and last equation of (16), we obtain

$$T_{s1}^\circ = \frac{\sigma_s I_s^\circ}{h_{s1}}, \quad T_{s2}^\circ = \frac{\sigma_s \sigma_{s1} I_s^\circ}{h_{s1} h_{s2}} \quad \text{and} \quad B^\circ = \frac{\phi_s I_s^\circ}{\mu_b - g}. \tag{17}$$

From the second equation of (16) we have

$$\left(\frac{\beta B^\circ}{B^\circ + k} + \frac{\beta_s I_s^\circ}{X^\circ + I_s^\circ + T_{s1}^\circ + T_{s2}^\circ} \right) X^\circ = h_s I_s^\circ. \tag{18}$$

Replacing the left hand side of (18) in the first equation of (16) we obtain

$$X^\circ = \frac{\Lambda - h_s I_s^\circ}{\mu}. \tag{19}$$

Substituting (17) and (19) into the second equation of (16) leads to the following third order polynomial of I_s^*

$$I_s^* (a_2 I_s^{*2} + a_1 I_s^* + a_0) = 0. \tag{20}$$

Solving (20) gives $I_s^* = 0$ which corresponds to the cholera-free equilibrium or

$$a_2 I_s^{*2} + a_1 I_s^* + a_0 = 0 \tag{21}$$

where

$$\begin{cases} a_0 &= \Lambda k \mu h_s h_{s1} h_{s2} (\mu_b - g) [(\mathcal{R}_{\mathcal{B}_s} + \mathcal{R}_{\mathcal{H}_s}) - 1], \\ a_1 &h_s (k \mu (g - \mu_b) (h_{s1} h_{s2} (\mu + \beta_s) + \mu \sigma_s (h_{s2} + \sigma_{s1})) - \Lambda (2\beta + \mu) h_{s1} h_{s2} \phi_s) \\ &+ k \mu h_s^2 h_{s1} h_{s2} (\mu_b - g) + \Lambda \mu \phi_s (\beta \sigma_s (h_{s2} + \sigma_{s1}) + h_{s1} h_{s2} (\beta + \beta_s)), \\ a_2 &= h_s \phi_s (h_{s1} h_{s2} ((\beta + \mu) h_s - \mu (\beta + \mu + \beta_s)) - \mu (\beta + \mu) \sigma_s (h_{s2} + \sigma_{s1})). \end{cases} \tag{22}$$

Equilibrium points are feasible only if the condition $a_1^2 \geq 4a_0a_2$ is satisfied. The various possible numbers of roots for the equation (21) are illustrated in Table 1 below.

We observe that the cholera-sensitive only system (16) can have a maximum number of two equilibrium points, which are possible for either $(\mathcal{R}_{\mathcal{B}_s} + \mathcal{R}_{\mathcal{H}_s}) > 1$ or $(\mathcal{R}_{\mathcal{B}_s} + \mathcal{R}_{\mathcal{H}_s}) < 1$. In the stability analysis section, we investigate the stability of the cholera-sensitive-only sub-system.

Cholera-resistant only equilibrium

In this section, we compute the cholera-resistant only equilibrium, denoted by, $\mathcal{C}^\bullet = (X^\bullet, I_r^\bullet, T_{r1}^\bullet, T_{r2}^\bullet, B^\bullet)$. This is obtained by setting $I_s = T_{s1} = T_{s2} = 0$ in system (2) and solving the following system of equations

$$\begin{cases} 0 &= \Lambda - \mu X^\bullet - \left(\frac{\beta B^\bullet}{B^\bullet + k} + \frac{\beta_r I_r^\bullet}{X^\bullet + I_r^\bullet + T_{r1}^\bullet + T_{r2}^\bullet} \right) X^\bullet, \\ 0 &= \left(\frac{\beta B^\bullet}{B^\bullet + k} + \frac{\beta_r I_r^\bullet}{X^\bullet + I_r^\bullet + T_{r1}^\bullet + T_{r2}^\bullet} \right) X^\bullet - h_r I_r^\bullet, \\ 0 &= \sigma_r I_r^\bullet - h_{r1} T_{r1}^\bullet, \\ 0 &= \sigma_{r1} T_{r1}^\bullet - h_{r2} T_{r2}^\bullet, \\ 0 &= g B^\bullet + \phi_r I_r^\bullet - \mu_b B^\bullet. \end{cases} \tag{23}$$

We observe that system (23) and system (16) have the same structure. Thus, the results obtained for system (16) can be applied to system (23) by changing the variable from s to r . Thus, we obtain the following third-order polynomial of I_r^*

$$I_r^* (b_2 I_r^{*2} + b_1 I_r^* + b_0) = 0. \tag{24}$$

Solving (24) gives $I_r^* = 0$ which corresponds to the cholera-free equilibrium or

$$b_2 I_r^{*2} + b_1 I_r^* + b_0 = 0 \tag{25}$$

where

$$\begin{cases} b_0 &= \Lambda k \mu h_r h_{r1} h_{r2} (\mu_b - g) [(\mathcal{R}_{\mathcal{B}_r} + \mathcal{R}_{\mathcal{H}_r}) - 1], \\ b_1 &h_r (k \mu (g - \mu_b) (h_{r1} h_{r2} (\mu + \beta_r) + \mu \sigma_r (h_{r2} + \sigma_{r1})) - \Lambda (2\beta + \mu) h_{r1} h_{r2} \phi_r) \\ &+ k \mu h_r^2 h_{r1} h_{r2} (\mu_b - g) + \Lambda \mu \phi_r (\beta \sigma_r (h_{r2} + \sigma_{r1}) + h_{r1} h_{r2} (\beta + \beta_r)), \\ b_2 &= h_r \phi_r (h_{r1} h_{r2} ((\beta + \mu) h_r - \mu (\beta + \mu + \beta_r)) - \mu (\beta + \mu) \sigma_r (h_{r2} + \sigma_{r1})). \end{cases} \tag{26}$$

Equilibrium points are feasible only if the condition $b_1^2 \geq 4b_0b_2$ is satisfied. The various possible number of roots for the equation (25) is illustrated in Table 2 below.

	$a_0 > 0$				$a_0 < 0$			
	$((\mathcal{R}_{\mathcal{B}_s} + \mathcal{R}_{\mathcal{H}_s}) > 1)$				$((\mathcal{R}_{\mathcal{B}_s} + \mathcal{R}_{\mathcal{H}_s}) < 1)$			
	$a_1 > 0$		$a_1 < 0$		$a_1 > 0$		$a_1 < 0$	
	$a_2 > 0$	$a_2 < 0$	$a_2 > 0$	$a_2 < 0$	$a_2 > 0$	$a_2 < 0$	$a_2 > 0$	$a_2 < 0$
$I_{s_i}^*$	0	1	2	1	1	2	1	0

Table 1. Number of possible equilibrium points for the sensitive only sub-system.

We observe that the cholera-resistant only system (23) can have a maximum number of two equilibrium points, which are possible for either $(\mathcal{R}_{\mathcal{B}_r} + \mathcal{R}_{\mathcal{H}_r}) > 1$ or $(\mathcal{R}_{\mathcal{B}_r} + \mathcal{R}_{\mathcal{H}_r}) < 1$. In the stability analysis section, we investigate the stability of the cholera-resistant-only sub-system.

Cholera-coexistence equilibrium

We now compute the cholera-coexistence equilibrium where both strains exist, denoted by,

$$\mathcal{C}^* = (X^*, I_s^*, T_{s1}^*, T_{s2}^*, I_r^*, T_{r1}^*, T_{r2}^*, B^*).$$

This is obtained by solving the following system of equations:

$$\begin{cases} 0 = \Lambda - (\mu + \mathcal{A}^*) X^*, \\ 0 = (f\lambda^* + \lambda_s^*) X^* - h_s I_s^*, \\ 0 = \sigma_s I_s^* - h_{s1} T_{s1}^*, \\ 0 = \sigma_{s1} T_{s1}^* - h_{s2} T_{s2}^*, \\ 0 = ((1-f)\lambda^* + \lambda_r^*) X^* - h_r I_r^*, \\ 0 = \sigma_r I_r^* - h_{r1} T_{r1}^*, \\ 0 = \sigma_{r1} T_{r1}^* - h_{r2} T_{r2}^*, \\ 0 = gB^* + \phi_s I_s^* + \phi_r I_r^* - \mu_b B^*. \end{cases} \tag{27}$$

The computation of the coexistence equilibrium is cumbersome. We hereby present the cholera coexistence equilibrium in terms of \mathcal{A}^* , λ^* , λ_s^* and λ_r^* .

Thus, we obtain the cholera-coexistence equilibrium $\mathcal{C}^* = (X^*, I_s^*, T_{s1}^*, T_{s2}^*, I_r^*, T_{r1}^*, T_{r2}^*, B^*)$ where

$$\begin{cases} X^* = \frac{\Lambda}{\mu + \mathcal{A}^*}, \quad I_s^* = \frac{\Lambda(f\lambda^* + \lambda_s^*)}{(\mu + \mathcal{A}^*)h_s}, \quad T_{s1}^* = \frac{\Lambda\sigma_s(f\lambda^* + \lambda_s^*)}{(\mu + \mathcal{A}^*)h_s h_{s1}}, \quad T_{s2}^* = \frac{\Lambda\sigma_s\sigma_{s1}(f\lambda^* + \lambda_s^*)}{(\mu + \mathcal{A}^*)h_s h_{s1} h_{s2}}, \\ I_r^* = \frac{\Lambda((1-f)\lambda^* + \lambda_r^*)}{(\mu + \mathcal{A}^*)h_r}, \quad T_{r1}^* = \frac{\Lambda\sigma_r((1-f)\lambda^* + \lambda_r^*)}{(\mu + \mathcal{A}^*)h_r h_{r1}}, \quad T_{r2}^* = \frac{\Lambda\sigma_r\sigma_{r1}((1-f)\lambda^* + \lambda_r^*)}{(\mu + \mathcal{A}^*)h_r h_{r1} h_{r2}}, \\ B^* = \frac{\Lambda(h_s\phi_r((1-f)\lambda^* + \lambda_r^*) + h_r\phi_s(f\lambda^* + \lambda_s^*))}{(\mu + \mathcal{A}^*)h_r h_s (\mu_b - g)}. \end{cases} \tag{28}$$

Stability analysis of cholera-persistent equilibrium points

We now investigate the stability of the cholera-sensitive-only equilibrium and the cholera-resistant-only equilibrium. We employ the centre manifold theory mentioned in Castillo-Chavez and Song⁴⁸. We avoid re-writing the theorem and refer readers to⁴⁸.

Stability of the cholera-sensitive only equilibrium

We determine the stability of the cholera-sensitive only equilibrium \mathcal{C}° in Ω . Consider the following system of equations obtained from system (2) by setting $I_r = T_{r1} = T_{r2} = 0$ in system (2)

	$b_0 > 0$				$b_0 < 0$			
	$((\mathcal{R}_{\mathcal{B}_r} + \mathcal{R}_{\mathcal{H}_r}) > 1)$				$((\mathcal{R}_{\mathcal{B}_r} + \mathcal{R}_{\mathcal{H}_r}) < 1)$			
	$b_1 > 0$		$b_1 < 0$		$b_1 > 0$		$b_1 < 0$	
	$b_2 > 0$	$b_2 < 0$	$b_2 > 0$	$b_2 < 0$	$b_2 > 0$	$b_2 < 0$	$b_2 > 0$	$b_2 < 0$
$I_{r_i}^*$	0	1	2	1	1	2	1	0

Table 2. Number of possible equilibrium points for the resistant-only sub-system.

$$\left\{ \begin{aligned} \frac{dX}{dt} &= \Lambda - \mu X - \left(\frac{\beta B}{B+k} + \frac{\beta_s I_s}{X + I_s + T_{s1} + T_{s2}} \right) X, \\ \frac{dI_s}{dt} &= \left(\frac{\beta B}{B+k} + \frac{\beta_s I_s}{X + I_s + T_{s1} + T_{s2}} \right) X - h_s I_s, \\ \frac{dT_{s1}}{dt} &= \sigma_s I_s - h_{s1} T_{s1}, \\ \frac{dT_{s2}}{dt} &= \sigma_{s1} T_{s1} - h_{s2} T_{s2}, \\ \frac{dB}{dt} &= gB + \phi_s I_s - \mu_b B. \end{aligned} \right. \tag{29}$$

Let us make the following change of variables: $X = x_1^s$, $I_s = x_2^s$, $T_{s1} = x_3^s$, $T_{s2} = x_4^s$, $B = x_5^s$, so that

$N = \sum_{n=1}^5 x_n^s$. We now use the vector notation $X^s = (x_1^s, x_2^s, x_3^s, x_4^s, x_5^s)^T$. Then, system (29) can be written in the form $\frac{dX^s}{dt} = F^s(t, x^s(t)) = (f_1^s, f_2^s, f_3^s, f_4^s, f_5^s)^T$, where

$$\left\{ \begin{aligned} \frac{dx_1^s}{dt} &= \Lambda - \mu x_1^s - \left(\frac{\beta x_5^s}{x_5^s + k} + \frac{\beta_s x_2^s}{x_1^s + x_2^s + x_3^s + x_4^s} \right) x_1^s = f_1^s, \\ \frac{dx_2^s}{dt} &= \left(\frac{\beta x_5^s}{x_5^s + k} + \frac{\beta_s x_2^s}{x_1^s + x_2^s + x_3^s + x_4^s} \right) x_1^s - h_s x_2^s = f_2^s, \\ \frac{dx_3^s}{dt} &= \sigma_s x_2^s - h_{s1} x_3^s = f_3^s, \\ \frac{dx_4^s}{dt} &= \sigma_{s1} x_3^s - h_{s2} x_4^s = f_4^s, \\ \frac{dx_5^s}{dt} &= g x_5^s + \phi_s x_2^s - \mu_b x_5^s = f_5^s. \end{aligned} \right. \tag{30}$$

We assume $\beta = \varepsilon \beta_s$, with $\varepsilon = 1$ implying the transmission parameters are equal, $0 < \varepsilon < 1$ implying $\beta < \beta_s$ and lastly, $\varepsilon > 1$ implies $\beta > \beta_s$. Choosing β_s as the bifurcation parameter, the condition $\mathcal{R}_{\mathcal{B}_s} + \mathcal{R}_{\mathcal{H}_s} = 1$ corresponds to

$$\beta_s = \beta_s^* = \frac{k\mu h_s (g - \mu_b)}{k\mu (g - \mu_b) - \Lambda \varepsilon \phi_s}. \tag{31}$$

The Jacobian matrix of system (29) at $\mathcal{C}_0^s = (x_1^{s0}, x_2^{s0}, x_3^{s0}, x_4^{s0}, x_5^{s0}) = \left(\frac{\Lambda}{\mu}, 0, 0, 0, 0 \right)$ when $\beta_s = \beta_s^*$ is given by

$$J^*(\mathcal{C}_0^s) = \begin{pmatrix} -\mu & -\beta_s^* & 0 & 0 & -\frac{\Lambda \varepsilon \beta_s^*}{k\mu} \\ 0 & \beta_s^* - h_s & 0 & 0 & \frac{\Lambda \varepsilon \beta_s^*}{k\mu} \\ 0 & \sigma_s & -h_{s1} & 0 & 0 \\ 0 & 0 & \sigma_{s1} & -h_{s2} & 0 \\ 0 & \phi_s & 0 & 0 & g - \mu_b \end{pmatrix}.$$

where h_s, h_{s1} and h_{s2} are defined as before. The eigenvalues of $J^*(\mathcal{C}_0^s)$ are

$$l_1^s = 0, \quad l_2^s = -\mu, \quad l_3^s = -h_{s1}, \quad l_4^s = -h_{s2}, \quad l_5^s = \frac{\Lambda \varepsilon \phi_s (\mu_b - g + h_s) + k\mu (g - \mu_b)^2}{k\mu (g - \mu_b) - \Lambda \varepsilon \phi_s}.$$

Thus, system (30), with $\beta_s = \beta_s^*$ has a simple eigenvalue. Hence the center manifold theory can be used to analyse the dynamics of system (29) near $\beta_s = \beta_s^*$. It can be shown that $J^*(\mathcal{C}_0^s)$, has a right eigenvector given by $w = (w_1, w_2, w_3, w_4, w_5)^T$, where

$$\begin{aligned} w_1 &= -h_s h_{s1} h_{s2} (\mu_b - g), & w_2 &= \mu h_{s1} h_{s2} (\mu_b - g), & w_3 &= \mu h_{s2} \sigma_s (\mu_b - g), \\ w_4 &= \mu \sigma_s \sigma_{s1} (\mu_b - g), & w_5 &= \mu h_{s1} h_{s2} \phi_s. \end{aligned}$$

Here, we note that $w_1 < 0$ and $w_i > 0$, $i = 2, 3, 4, 5$. Further, the left eigenvector of $J^*(\mathcal{C}_0^s)$, associated with the zero eigenvalue at $\beta_s = \beta_s^*$ is given by $v = (v_1, v_2, v_3, v_4, v_5)^T$, where

$$v_1 = 0, \quad v_2 = k\mu\mu_b + \Lambda\epsilon\phi_s - gk\mu, \quad v_3 = v_4 = 0 \quad \text{and} \quad v_5 = \Lambda\epsilon h_s.$$

The computations of **a** and **b** are necessary in order to apply Theorem 4.1 in Castillo-Chavez and Song⁴⁸. For system (30), the associated non-zero partial derivatives of F^{s^*} at $\mathcal{C}_0^{s^*}$ are given in (32).

$$\begin{aligned} \frac{\partial^2 f_1^s}{\partial x_1^s \partial x_5^s} &= \frac{\partial^2 f_1^s}{\partial x_3^s \partial x_1^s} = -\frac{\epsilon\beta_s}{k}, & \frac{\partial^2 f_1^s}{\partial x_2^s \partial x_5^s} &= \frac{\partial^2 f_1^s}{\partial x_2^s \partial x_3^s} = \frac{2\mu\beta_s}{\Lambda}, & \frac{\partial^2 f_1^s}{\partial x_2^s \partial x_3^s} &= \frac{\partial^2 f_1^s}{\partial x_3^s \partial x_2^s} = \frac{\mu\beta_s}{\Lambda}, \\ \frac{\partial^2 f_1^s}{\partial x_2^s \partial x_4^s} &= \frac{\partial^2 f_1^s}{\partial x_4^s \partial x_2^s} = \frac{\mu\beta_s}{\Lambda}, & \frac{\partial^2 f_1^s}{\partial x_3^s \partial x_5^s} &= \frac{\partial^2 f_1^s}{\partial x_5^s \partial x_3^s} = \frac{2\Lambda\epsilon\beta_s}{k^2\mu}, & \frac{\partial^2 f_2^s}{\partial x_1^s \partial x_5^s} &= \frac{\partial^2 f_2^s}{\partial x_5^s \partial x_1^s} = \frac{\epsilon\beta_s}{k}, \\ \frac{\partial^2 f_2^s}{\partial x_2^s \partial x_2^s} &= \frac{\partial^2 f_2^s}{\partial x_2^s \partial x_2^s} = -\frac{2\mu\beta_s}{\Lambda}, & \frac{\partial^2 f_2^s}{\partial x_3^s \partial x_3^s} &= \frac{\partial^2 f_2^s}{\partial x_3^s \partial x_2^s} = -\frac{\mu\beta_s}{\Lambda}, & \frac{\partial^2 f_2^s}{\partial x_2^s \partial x_4^s} &= \frac{\partial^2 f_2^s}{\partial x_4^s \partial x_2^s} = -\frac{\mu\beta_s}{\Lambda}, \\ \frac{\partial^2 f_2^s}{\partial x_5^s \partial x_5^s} &= \frac{\partial^2 f_2^s}{\partial x_5^s \partial x_5^s} = -\frac{2\Lambda\epsilon\beta_s}{k^2\mu}, & \frac{\partial^2 f_1^s}{\partial x_2^s \partial \beta_s^*} &= -1, & \frac{\partial^2 f_1^s}{\partial x_3^s \partial \beta_s^*} &= -\frac{\Lambda\epsilon}{k\mu}, & \frac{\partial^2 f_2^s}{\partial x_2^s \partial \beta_s^*} &= 1, & \frac{\partial^2 f_2^s}{\partial x_5^s \partial \beta_s^*} &= \frac{\Lambda\epsilon}{k\mu}. \end{aligned} \tag{32}$$

It thus follows that

$$\begin{aligned} \mathbf{a} &= v_2 w_1 w_5 \frac{\partial^2 f_2^s}{\partial x_1^s \partial x_5^s} + v_2 w_5 w_1 \frac{\partial^2 f_2^s}{\partial x_5^s \partial x_1^s} + v_2 w_2 w_3 \frac{\partial^2 f_2^s}{\partial x_2^s \partial x_3^s} + v_2 w_3 w_2 \frac{\partial^2 f_2^s}{\partial x_3^s \partial x_2^s} \\ &= v_2 w_2 w_2 \frac{\partial^2 f_2^s}{\partial x_2^s \partial x_2^s} + v_2 w_2 w_4 \frac{\partial^2 f_2^s}{\partial x_2^s \partial x_4^s} + v_2 w_4 w_2 \frac{\partial^2 f_2^s}{\partial x_4^s \partial x_2^s} + v_2 w_5 w_5 \frac{\partial^2 f_2^s}{\partial x_5^s \partial x_5^s} \\ &= \left(\frac{-2\mu h_{s1} h_{s2} \beta_s (k\mu(\mu_b - g) + \Lambda\epsilon\phi_s)}{k^2\Lambda} \right) \times \\ &\quad \left[k^2\mu^2 (\mu_b - g)^2 (\sigma_s (h_{s2} + \sigma_{s1}) + h_{s1} h_{s2}) + k\Lambda\epsilon h_s h_{s1} h_{s2} \phi_s (\mu_b - g) + \Lambda^2 \epsilon h_{s1} h_{s2} \phi_s^2 \right] < 0 \quad \text{and} \\ \mathbf{b} &= v_2 w_2 \frac{\partial^2 f_2^s}{\partial x_2^s \partial \beta_s^*} + v_2 w_5 \frac{\partial^2 f_2^s}{\partial x_5^s \partial \beta_s^*} = \frac{h_{s1} h_{s2} (k\mu\mu_b - gk\mu + \Lambda\epsilon\phi_s)^2}{k} > 0. \end{aligned}$$

We thus have the following result

Theorem 3 Since $\mathbf{a} < 0$ and $\mathbf{b} > 0$, the cholera sensitive equilibrium \mathcal{C}° is locally asymptotically stable for $(\mathcal{R}_{\mathcal{B}_s} + \mathcal{R}_{\mathcal{H}_s}) > 1$ but close to one.

Stability of the cholera-resistant only equilibrium

We determine the stability of the cholera-resistant only equilibrium \mathcal{C}^* in Ω . Consider the following system of equations obtained from system (2) by setting $I_s = T_{s1} = T_{s2} = 0$ in system (2)

$$\begin{cases} \frac{dX}{dt} = \Lambda - \mu X - \left(\frac{\beta B}{B+k} + \frac{\beta_r I_r}{X + I_r + T_{r1} + T_{r2}} \right) X, \\ \frac{dI_r}{dt} = \left(\frac{\beta B}{B+k} + \frac{\beta_r I_r}{X + I_r + T_{r1} + T_{r2}} \right) X - h_r I_r, \\ \frac{dT_{r1}}{dt} = \sigma_r I_r - h_{r1} T_{r1}, \\ \frac{dT_{r2}}{dt} = \sigma_{r1} T_{r1} - h_{r2} T_{r2}, \\ \frac{dB}{dt} = gB + \phi_r I_r - \mu_b B. \end{cases} \tag{33}$$

Let us make the following change of variables: $X = x_1^r$, $I_r = x_2^r$, $T_{r1} = x_3^r$, $T_{r2} = x_4^r$, $B = x_5^r$, so that

$N = \sum_{n=1}^5 x_n^r$. We now use the vector notation $X^r = (x_1^r, x_2^r, x_3^r, x_4^r, x_5^r)^T$. Then, system (33) can be written in the form $\frac{dX^r}{dt} = F^r(t, x^r(t)) = (f_1^r, f_2^r, f_3^r, f_4^r, f_5^r)^T$, where

$$\begin{cases} \frac{dx_1^r}{dt} = \Lambda - \mu x_1^r - \left(\frac{\beta x_5^r}{x_5^r + k} + \frac{\beta_r x_2^r}{x_1^r + x_2^r + x_3^r + x_4^r} \right) x_1^r = f_1^r, \\ \frac{dx_2^r}{dt} = \left(\frac{\beta x_5^r}{x_5^r + k} + \frac{\beta_r x_2^r}{x_1^r + x_2^r + x_3^r + x_4^r} \right) x_1^r - h_r x_2^r = f_2^r, \\ \frac{dx_3^r}{dt} = \sigma_r x_2^r - h_{r1} x_3^r = f_3^r, \\ \frac{dx_4^r}{dt} = \sigma_{r1} x_3^r - h_{r2} x_4^r = f_4^r, \\ \frac{dx_5^r}{dt} = g x_5^r + \phi_r x_2^r - \mu_b x_5^r = f_5^r. \end{cases} \tag{34}$$

We assume $\beta = \varepsilon \beta_r$, with $\varepsilon = 1$ implying the transmission parameters are equal, $0 < \varepsilon < 1$ implying $\beta < \beta_r$ and lastly, $\varepsilon > 1$ implies $\beta > \beta_r$. Choosing β_r as the bifurcation parameter, the condition $\mathcal{R}_{\mathcal{B}_r} + \mathcal{R}_{\mathcal{H}_r} = 1$ corresponds to

$$\beta_r = \beta_r^* = \frac{k\mu h_r (g - \mu_b)}{k\mu (g - \mu_b) - \Lambda \varepsilon \phi_r}. \tag{35}$$

The Jacobian matrix of system (33) at $\mathcal{C}_0^r = (x_1^{r0}, x_2^{r0}, x_3^{r0}, x_4^{r0}, x_5^{r0}) = \left(\frac{\Lambda}{\mu}, 0, 0, 0, 0 \right)$ when $\beta_r = \beta_r^*$ is given by

$$J^*(\mathcal{C}_0^r) = \begin{pmatrix} -\mu & -\beta_r^* & 0 & 0 & -\frac{\Lambda \varepsilon \beta_r^*}{k\mu} \\ 0 & \beta_r^* - h_r & 0 & 0 & \frac{\Lambda \varepsilon \beta_r^*}{k\mu} \\ 0 & \sigma_r & -h_{r1} & 0 & 0 \\ 0 & 0 & \sigma_{r1} & -h_{r2} & 0 \\ 0 & \phi_r & 0 & 0 & g - \mu_b \end{pmatrix}.$$

where h_r, h_{r1} and h_{r2} are defined as before. The eigenvalues of $J^*(\mathcal{C}_0^r)$ are

$$l_1^r = 0, \quad l_2^r = -\mu, \quad l_3^r = -h_{r1}, \quad l_4^r = -h_{r2}, \quad l_5^r = \frac{\Lambda \varepsilon \phi_r (\mu_b - g + h_r) + k\mu (g - \mu_b)^2}{k\mu (g - \mu_b) - \Lambda \varepsilon \phi_r}.$$

Thus, system (34), with $\beta_r = \beta_r^*$ has a simple eigenvalue. Hence the center manifold theory can be used to analyse the dynamics of system (33) near $\beta_r = \beta_r^*$. It can be shown that $J^*(\mathcal{C}_0^r)$, has a right eigenvector given by $\omega = (\omega_1, \omega_2, \omega_3, \omega_4, \omega_5)^T$, where

$$\begin{aligned} \omega_1 &= -h_r h_{r1} h_{r2} (\mu_b - g), & \omega_2 &= \mu h_{r1} h_{r2} (\mu_b - g), & \omega_3 &= \mu h_{r2} \sigma_r (\mu_b - g), \\ \omega_4 &= \mu \sigma_r \sigma_{r1} (\mu_b - g), & \omega_5 &= \mu h_{r1} h_{r2} \phi_r. \end{aligned}$$

Here, we note that $\omega_1 < 0$ and $\omega_i > 0, \quad i = 2, 3, 4, 5$. Further, the left eigenvector of $J^*(\mathcal{C}_0^r)$, associated with the zero eigenvalue at $\beta_r = \beta_r^*$ is given by $\nu = (\nu_1, \nu_2, \nu_3, \nu_4, \nu_5)^T$, where

$$\nu_1 = 0, \quad \nu_2 = k\mu\mu_b + \Lambda \varepsilon \phi_r - gk\mu, \quad \nu_3 = \nu_4 = 0 \quad \text{and} \quad \nu_5 = \Lambda \varepsilon h_r.$$

The computations of **a** and **b** are necessary in order to apply Theorem 4.1 in Castillo-Chavez and Song⁴⁸. For system (34), the associated non-zero partial derivatives of F^r at \mathcal{C}_0^r are given in (36).

$$\begin{aligned} \frac{\partial^2 f_1^r}{\partial x_1^r \partial x_5^r} &= \frac{\partial^2 f_1^r}{\partial x_5^r \partial x_1^r} = -\frac{\varepsilon \beta_r}{k}, & \frac{\partial^2 f_1^r}{\partial x_2^r \partial x_2^r} &= \frac{\partial^2 f_1^r}{\partial x_2^r \partial x_2^r} = \frac{2\mu \beta_r}{\Lambda}, & \frac{\partial^2 f_1^r}{\partial x_3^r \partial x_3^r} &= \frac{\partial^2 f_1^r}{\partial x_3^r \partial x_3^r} = \frac{\mu \beta_r}{\Lambda}, \\ \frac{\partial^2 f_1^r}{\partial x_2^r \partial x_4^r} &= \frac{\partial^2 f_1^r}{\partial x_4^r \partial x_2^r} = \frac{\mu \beta_r}{\Lambda}, & \frac{\partial^2 f_1^r}{\partial x_5^r \partial x_5^r} &= \frac{\partial^2 f_1^r}{\partial x_5^r \partial x_5^r} = \frac{2\Lambda \varepsilon \beta_r}{k^2 \mu}, & \frac{\partial^2 f_2^r}{\partial x_1^r \partial x_5^r} &= \frac{\partial^2 f_2^r}{\partial x_5^r \partial x_1^r} = \frac{\varepsilon \beta_r}{k}, \\ \frac{\partial^2 f_2^r}{\partial x_2^r \partial x_2^r} &= \frac{\partial^2 f_2^r}{\partial x_2^r \partial x_2^r} = -\frac{2\mu \beta_r}{\Lambda}, & \frac{\partial^2 f_2^r}{\partial x_2^r \partial x_3^r} &= \frac{\partial^2 f_2^r}{\partial x_3^r \partial x_2^r} = -\frac{\mu \beta_r}{\Lambda}, & \frac{\partial^2 f_2^r}{\partial x_2^r \partial x_4^r} &= \frac{\partial^2 f_2^r}{\partial x_4^r \partial x_2^r} = -\frac{\mu \beta_r}{\Lambda}, \\ \frac{\partial^2 f_2^r}{\partial x_5^r \partial x_5^r} &= \frac{\partial^2 f_2^r}{\partial x_5^r \partial x_5^r} = -\frac{2\Lambda \varepsilon \beta_r}{k^2 \mu}, & \frac{\partial^2 f_1^r}{\partial x_2^r \partial \beta_r^*} &= -1, & \frac{\partial^2 f_1^r}{\partial x_5^r \partial \beta_r^*} &= -\frac{\Lambda \varepsilon}{k\mu}, & \frac{\partial^2 f_2^r}{\partial x_2^r \partial \beta_r^*} &= 1, & \frac{\partial^2 f_2^r}{\partial x_5^r \partial \beta_r^*} &= \frac{\Lambda \varepsilon}{k\mu}. \end{aligned} \tag{36}$$

It thus follows that

$$\begin{aligned}
 a &= \nu_2\omega_1\omega_5 \frac{\partial^2 f_2^r}{\partial x_1^r \partial x_5^r} + \nu_2\omega_5\omega_1 \frac{\partial^2 f_2^r}{\partial x_5^r \partial x_1^r} + \nu_2\omega_2\omega_3 \frac{\partial^2 f_2^r}{\partial x_2^r \partial x_3^r} + \nu_2\omega_3\omega_2 \frac{\partial^2 f_2^r}{\partial x_3^r \partial x_2^r} \\
 &= \nu_2\omega_2\omega_2 \frac{\partial^2 f_2^r}{\partial x_2^r \partial x_2^r} + \nu_2\omega_2\omega_4 \frac{\partial^2 f_2^r}{\partial x_2^r \partial x_4^r} + \nu_2\omega_4\omega_2 \frac{\partial^2 f_2^r}{\partial x_4^r \partial x_2^r} + \nu_2\omega_5\omega_5 \frac{\partial^2 f_2^r}{\partial x_5^r \partial x_5^r} \\
 &= \left(\frac{-2\mu h_{r1} h_{r2} \beta_r (k\mu (\mu_b - g) + \Lambda \epsilon \phi_r)}{k^2 \Lambda} \right) \times \\
 &\quad \left[k^2 \mu^2 (\mu_b - g)^2 (\sigma_r (h_{r2} + \sigma_{r1}) + h_{r1} h_{r2}) + k \Lambda \epsilon h_r h_{r1} h_{r2} \phi_r (\mu_b - g) + \Lambda^2 \epsilon h_{r1} h_{r2} \phi_r^2 \right] < 0 \quad \text{and} \\
 b &= \nu_2\omega_2 \frac{\partial^2 f_2^r}{\partial x_2^r \partial \beta_r^*} + \nu_2\omega_5 \frac{\partial^2 f_2^r}{\partial x_5^r \partial \beta_r^*} = \frac{h_{r1} h_{r2} (k\mu \mu_b - gk\mu + \Lambda \epsilon \phi_r)^2}{k} > 0.
 \end{aligned}$$

We thus have the following result

Theorem 4 *Since $a < 0$ and $b > 0$, the cholera resistant equilibrium \mathcal{C}^* is locally asymptotically stable for $(\mathcal{R}_{\mathcal{B}^*} + \mathcal{R}_{\mathcal{H}^*}) > 1$ but close to one.*

Numerical simulations

This section presents the outcomes of the numerical simulations conducted on the model (2). The initial conditions used to obtain the results are as follows: $X(0) = 99980$, $I_s(0) = 200$, $T_{s1}(0) = 200$, $T_{s2}(0) = 200$, $I_r(0) = 200$, $T_{r1}(0) = 200$, $T_{r2}(0) = 200$, $Q(0) = 200$, $B(0) = 40000$. The table below shows the parameters used to generate the numerical results.

Markov Chain Monte Carlo and Stan

Markov Chain Monte Carlo (MCMC) methods have become indispensable tools in statistical modelling and Bayesian inference. Among the various MCMC algorithms, Stan, a probabilistic programming language and inference engine, has gained prominence for its efficiency, flexibility, and user-friendly interface. This subsection aims to provide an overview of the key developments, applications, and comparisons of Stan and MCMC methods in the field of statistics, data analysis, and mathematical biology.

MCMC methods have become foundational in Bayesian statistics, allowing for the estimation of complex posterior distributions in various applications. Early works by Metropolis et al.⁵³ and Hastings⁵⁴ laid the groundwork for MCMC, while the seminal paper by Gelfand and Smith⁵⁵ demonstrated its application in Bayesian analysis. The Gibbs sampling algorithm (Geman and Geman,⁵⁶) and the Metropolis-Hastings algorithm (Metropolis et al.,⁵³; Hastings,⁵⁴) are fundamental components of MCMC.

Stan, is a high-level probabilistic programming language designed for specifying Bayesian models. It leverages the No-U-Turn Sampler (NUTS) algorithm, an adaptive Hamiltonian Monte Carlo (HMC) method (Hoffman and Gelman,⁵⁷). Stan provides an expressive language for model specification, offering a balance between simplicity and flexibility. The declarative nature of Stan code facilitates model building and allows users to focus on the statistical aspects of their analysis. Stan’s popularity can be attributed to several advantages. Firstly, it provides automatic differentiation, enabling efficient gradient-based sampling. The NUTS algorithm, implemented in Stan, exhibits superior convergence properties compared to traditional MCMC algorithms, such as Gibbs sampling or Metropolis-Hastings. Additionally, Stan offers a wide range of built-in probability distributions, making it easy to specify complex models.

While Stan has numerous virtues, it is not without challenges. The versatility of Stan is evident in its successful application across various domains. Examples include Caughey et al.⁵⁸ in epidemiology, Vehtari et al.⁵⁹ in finance, and Carpenter et al.⁶⁰ in machine learning. Application in hierarchical modeling and large-scale data analysis has been particularly notable (Betancourt and Girolami,⁶¹). The challenges of the language range from struggling with the computational demands of some models, to obtaining divergent chains in the simulations. Ongoing research aims to address these challenges and improve the scalability and efficiency of Stan for large and complex datasets and models.

Table 3 is populated by parameters that are sourced from the literature and by parameters that are obtained from the application of MCMC and Stan. The dataset used in the application of MCMC and Stan was sourced from the website *Data.world*⁶². The dataset contains the number of cholera cases and related deaths, tracked monthly from October 31, 2010 to March 30, 2016 in Haiti.

Model trajectories

In this subsection, we document and analyse the trajectories of each of the infectious classes. The following figures show the fixed points of all the infectious classes under varying conditions. Using numerical simulation, we verify the results obtained in Section “Cholera-persistent equilibrium points”.

Figure 2 shows the cholera-sensitive-only equilibrium. The equilibrium point $\mathcal{C}^\diamond = (X^\diamond, I_s^\diamond, T_{s1}^\diamond, T_{s2}^\diamond, B^\diamond)$ is obtained by setting all the resistance classes to zero ($I_r = T_{r1} = T_{r2} = 0$). Figure 2 is partitioned into two parts. The bottom partition of Fig. 2 shows the range of the I_s class limited to the lowest 1000 values. The rest of the values of the range of I_s are shown in the top partition. The x and the y axis capture time in days and the I_s class, respectively. The opacity of the points and the size of the points capture the remaining two sensitive classes, T_{s2} and T_{s1} , respectively. From the first key, we note that a small-sized dot is associated with a low value for T_{s1}

and a large sized dot is associated with a large-value for T_{s1} . The second key shows that a fully transparency dot denotes a low value for the variable T_{s2} , whilst a non-transparent dot denotes a high value for the variable T_{s2} .

Similarly, the cholera-resistant-only equilibrium is found graphically in Fig. 3. The equilibrium point $\mathcal{C}^\bullet = (X^\bullet, I_r^\bullet, T_{r1}^\bullet, T_{r2}^\bullet, B^\bullet)$ is obtained by setting all the sensitive classes to zero ($I_s = T_{s1} = T_{s2} = 0$). The bottom partition of Fig. 3 shows the range of the I_r class limited to the lowest 1000 values. The rest of the values of the range of I_r are shown in the top partition. The x and the y axis capture time in days and the I_r class, respectively. The opacity of the points and the size of the points capture the remaining two resistant classes, T_{r2} and T_{r1} , respectively. From the first key, we note that a small-sized dot is associated with a low value for T_{r1} and a large sized dot is associated with a large-value for T_{r1} . The second key shows that a fully transparency dot denotes a low value for the variable T_{r2} , whilst a non-transparent dot denotes a high value for the variable T_{r2} .

Similarly, the cholera-persistent equilibrium is found graphically in Fig. 4. The equilibrium point $\mathcal{C}^* = (X^*, I_s^*, T_{s1}^*, T_{s2}^*, I_r^*, T_{r1}^*, T_{r2}^*, B^*)$, is obtained by setting all the derivatives of the state variables to zero. The bottom partition of Fig. 4 shows the range of the I_r and I_s classes limited to the lowest 1000 values. The rest of the values of the I_s and I_r range are shown in the top partition. The x and the y axis capture time in days and the I_r (red) and I_s (blue) classes, respectively. The opacity of the points and the size of the points capture the remaining two resistant classes, T_{s2} and T_{s1} , respectively. From the top key, we observe that the colour of the dot denotes the sensitivity of the strain of cholera. That is, the sensitive strain trajectories are shown in blue, whilst the resistant strain trajectories are shown in red. The middle key demonstrates that a small-sized dot represents a low value for T_{r1} or T_{s1} , whilst a large sized dot represents a large value for T_{r1} or T_{s1} . The bottom key shows that a fully transparency dot denotes a low value for the variable T_{r2} or T_{s2} , whilst a non-transparent dot denotes a high value for the variable T_{r2} or T_{s2} .

In Figs. 2, 3, 4, it can be observed that the fixed points to the classes I_r and I_s are established in the bottom partitions of each of these figures. It is further observed that, in the top partitions of each figure, the right tails of all the graphs consist of points with constant size and opacity. This observation suggests that the classes T_{s1} , T_{s2} , T_{r1} , and T_{r2} reach their respective equilibria in each of these figures. These findings are consistent with the results obtained in Section “Cholera-persistent equilibrium points”.

We observe that the size of the points in Fig. 5 decreases when curve’s peak is reached. This means that the number of people infected with the resistant strain of cholera significantly decreases when those people enter the second line of treatment. It is further observed that the size of the points in Fig. 6 do not decrease when

Par.	Range	Point value	Source
β_s		8.4	Calculated
Λ		16.34	Calculated
μ	(0.1–1)	0.02	49
θ_s		0.4	Calculated
δ_s	(0.240–4.662)	0.39	50,51
β	(0.15–1.5)	0.5	25,49,52
κ	($10^6 - 10^9$)	10^6	25,50,52
ϕ_s	(10–50)	50	25,50
μ_b	(0.03–0.034)	0.03	25,50,52
g	(0 – 10)	0.0073	49
σ_s	(0.20619–0.5)	0.20619	26
σ_{s1}		0.20619	Calculated
δ_{s1}		0.39	Calculated
δ_{s2}		0.39	Calculated
θ_{s1}		0.4	Calculated
θ_{s2}		0.4	Calculated
β_r		8.4	Calculated
ϕ_r	(10–50)	50	50,51
θ_r		0.4	Calculated
θ_{r1}	(0.017–0.5)	0.4	Calculated
θ_{r2}		0.4	Calculated
δ_r	(0.240–4.662)	0.39	50,51
δ_{r1}		0.39	Calculated
δ_{r2}	(0.07–0.245)	0.39	Calculated
σ_r	(0.20619–0.5)	0.20619	26
σ_{r1}		0.20619	Calculated

Table 3. Parameter values and their sources.

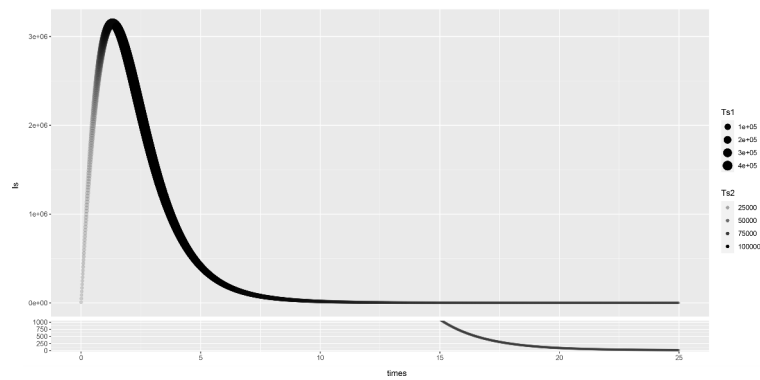


Fig. 2. The trajectories of the sensitive-strain classes, I_s , T_{s1} , T_{s2} . The size of the points tracks the T_{s1} and the opacity of the point tracks the T_{s2} .

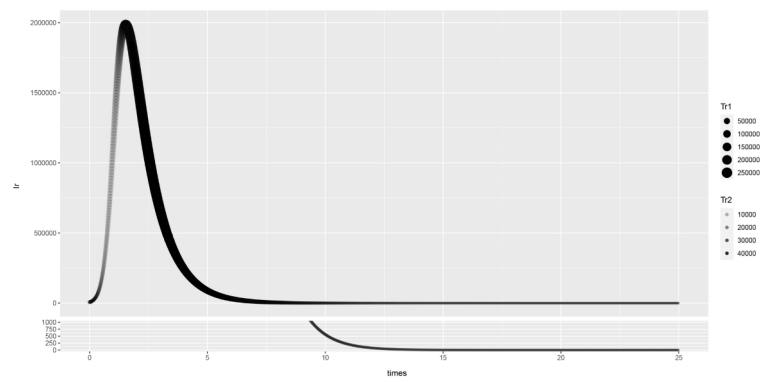


Fig. 3. The trajectories of the resistant-strain classes, I_r , T_{r1} , T_{r2} . The size of the points tracks the T_{r1} and the opacity of the point tracks the T_{r2} .

the curve reaches its peak. This suggests that a second line of treatment is redundant for the sensitive strain of cholera. These observations underscore the importance for a second line of treatment in the presence of a resistant strain of cholera. Furthermore, these results also suggest that as strains become progressively resistant, the management of cholera would also need to increase the lines of treatment. The latter observation will require further investigation in a future paper.

Latin hyper cube sampling (LHS) and partial rank correlation coefficient (PRCC)

In this subsection, we apply two statistical methods to perform a sensitivity analysis of model 2: Latin Hypercube Sampling (LHS) and Partial Rank Correlation Coefficient (PRCC). LHS, introduced by McKay et al. in 1979⁶³, is a robust technique for exploring parameter space, while PRCC, developed by Spearman in 1904⁶⁴, is used to assess the correlation between model inputs and outputs. Figure 7 highlights the most sensitive parameters in model 2, focusing on individuals infected with the resistant strain of cholera, I_r , and those infected with the sensitive strain, I_s .

The positive correlation between β and I_r is shown in Fig. 7a, whilst the negative correlation between δ_s , μ , θ_s , θ_{s1} , θ_{s2} , and I_r is shown in Fig. 7b–f, respectively. Figure 7g shows that μ and I_s are negatively correlated, while Fig. 7h shows that θ_r and I_s are positively correlated. The p -values of the remaining parameters of model 2 were all above 0.05. This finding implies that the remaining parameters are weakly correlated to the state variables I_r and I_s .

Discussion

In this paper, we developed and analyzed an antibiotic resistance cholera epidemic model with stage-switching of two antibiotics. We established and validated the equilibrium points of the cholera sensitive-only model, the cholera resistant-only model, and the cholera coexistence model through numerical simulations. Our analysis demonstrated the stability of all equilibrium points, and sensitivity analysis revealed that the most influential parameters include β , δ_s , μ , θ_s , θ_{s1} , θ_{s2} , and θ_r . Figure 4 illustrates that the resistant strain of cholera is the primary driver of the infection. This finding highlights the critical importance of managing the resistant strain to effectively reduce infection rates. Therefore, the judicious use of antibiotics, particularly those that are new and have broad-spectrum activity, is essential to mitigate and, in some cases, prevent the emergence of antimicrobial resistance. The PRCC diagrams (Fig. 7) show that six out of the eight most sensitive parameters are linked to

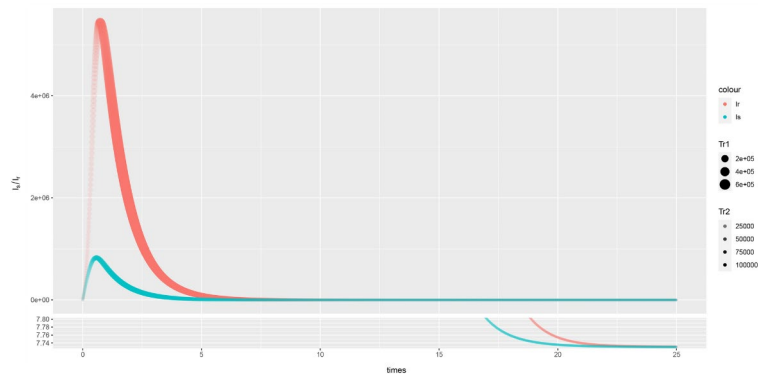


Fig. 4. The trajectories of both sensitive-strain and resistant-strain classes, I_s , T_{s1} , T_{s2} , I_r , T_{r1} , T_{r2} . The size of the points track T_{r1} (red) and T_{s1} (blue) and the opacity of the points track T_{r2} (red) and (blue) T_{s2} .

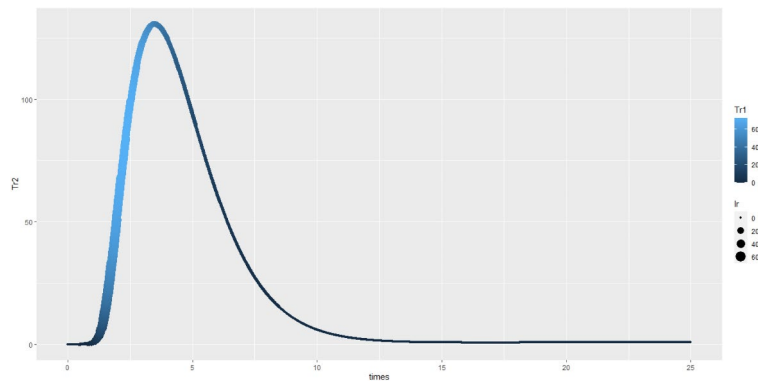


Fig. 5. A graph showing the number of cholera cases under treatment due to infection by the resistant strain over time.

the resistant strain of cholera, I_r . This indicates that targeted intervention strategies should prioritize these parameters to minimize the spread of resistant cholera strains.

In this study, we analyze the dynamics of a cholera model with stage switching. Stage switching is the process of subjecting cholera-infected individuals who experience treatment failure (due to resistance) to an alternative course of treatment. In some instances, the second-line drugs tend to be more expensive, more toxic (or both) than first-line drugs. This means that the course of drugs must be administered consecutively. Simulations on our model show that in the presence of a resistant strain of cholera, the use of second-line drugs is necessary for the management of cholera. This is exemplified by the observed inverse correlation between the number of MDR cases of cholera and the number of cases that receive the second-line drug treatment. To avoid treatment failure, our study highlights the necessity for stringent public health policies regarding antibiotic stewardship. Policymakers should promote guidelines that ensure the rational prescription and use of antibiotics to prevent the emergence and spread of resistant strains. In addition, public health campaigns aimed at educating healthcare providers and the general public about the dangers of inappropriate antibiotic use are crucial. Surveillance systems should be strengthened to monitor antibiotic resistance patterns and to inform timely interventions. The implementation of regulations that restrict the over-the-counter sale of antibiotics and enforce strict infection control measures in healthcare settings can also contribute to reducing the burden of antibiotic-resistant cholera.

This study can be extended by incorporating additional complexities into the model. For instance, the model can be refined to include resistance to second-line drugs, which is a growing concern due to increased reliance on these drugs in treating resistant bacterial infections. Future studies could investigate the impact of various antibiotic-switching strategies, such as random versus directed switching, and assess their cost-effectiveness in different epidemiological contexts. Another potential extension is to model the emergence of resistance to third-line and fourth-line drugs, which may become necessary as resistance to existing antibiotics escalates. Additionally, integrating socio-economic factors, such as healthcare access and affordability, into the model could provide a more comprehensive understanding of the dynamics of antibiotic resistance in cholera epidemics. Exploring the effects of global climate change on the transmission dynamics of cholera and the subsequent impact on antibiotic resistance patterns could also be a valuable research direction.

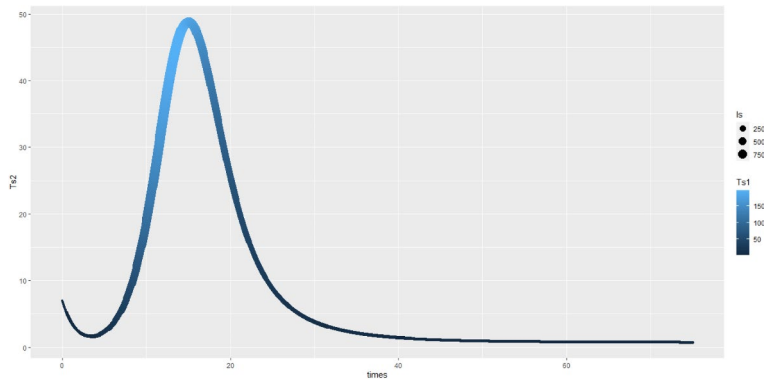


Fig. 6. A graph showing the number of cholera cases under treatment due to infection by the sensitive strain over time.

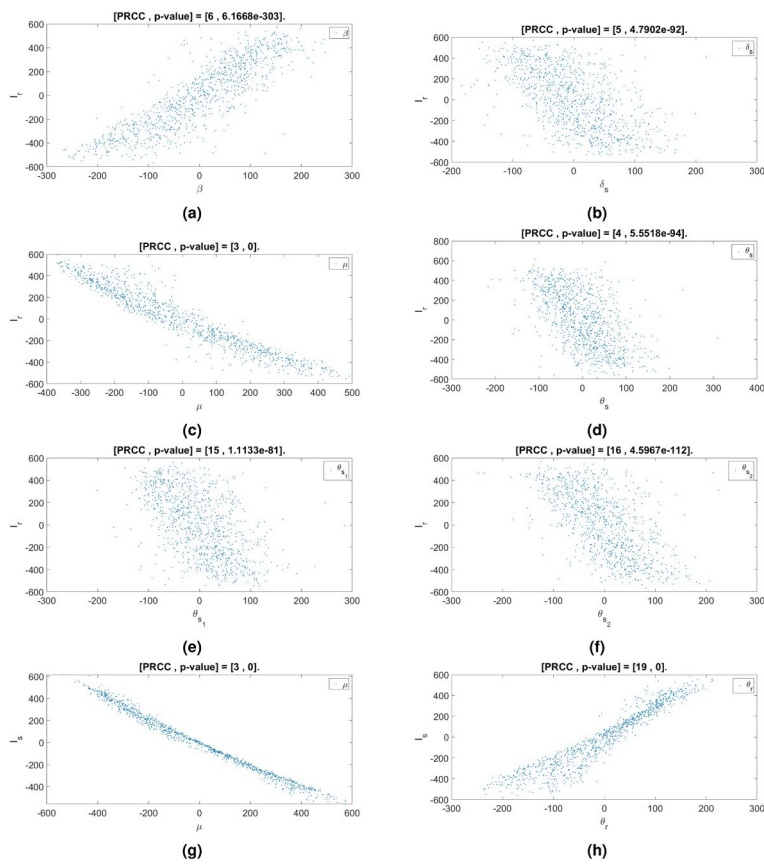


Fig. 7. PRCC plots of the most sensitive parameters, and the individuals infected with the resistant strain of cholera, I_r , and individuals infected with the sensitive strain of cholera, I_s .

Data availability

All data generated or analysed during this study are included in this published article.

Received: 29 March 2024; Accepted: 25 October 2024

Published online: 03 December 2024

References

1. Koelle, K., Pascual, M. & Yunus, M. Serotype cycles in cholera dynamics. *Proc. Royal Soc. B: Biol. Sci.* **273**, 2879–2886 (2006).
2. World Health Organization. Cholera (2023). Accessed: 2024-09-29.
3. Kaper, J. B., Morris, J. G. & Levine, M. M. Cholera. *Clin. Microbiol. Rev.* **8**, 48–86 (1995).

4. Ali, M., Nelson, A. R., Lopez, A. L. & Sack, D. A. Updated global burden of cholera in endemic countries. *PLoS Negl. Trop. Dis.* **9**, e0003832 (2015).
5. European Centre for Disease Prevention and Control. Cholera - surveillance and disease data: Cholera monthly (2024). Accessed: 2024-09-29.
6. Organization, W. H. et al. Who report on surveillance of antibiotic consumption: 2016-2018 early implementation. (2018).
7. Tacconelli, E. et al. Discovery, research, and development of new antibiotics: The who priority list of antibiotic-resistant bacteria and tuberculosis. *Lancet Infect. Dis.* **18**, 318–327 (2018).
8. Organization, W. H. et al. *Prioritization of Pathogens to Guide Discovery, Research and Development of New Antibiotics for Drug-Resistant Bacterial Infections, Including Tuberculosis* (World Health Organization, Tech. Rep., 2017).
9. Boucher, H. W. et al. Bad bugs, no drugs: No escape! an update from the infectious diseases society of america. *Clin. Infect. Dis.* **48**, 1–12 (2009).
10. Watts, J. E., Schreier, H. J., Lanska, L. & Hale, M. S. The rising tide of antimicrobial resistance in aquaculture: Sources, sinks and solutions. *Mar. Drugs* **15**, 158 (2017).
11. Verma, J. et al. Genomic plasticity associated with antimicrobial resistance in vibrio cholerae. *Proc. Natl. Acad. Sci.* **116**, 6226–6231 (2019).
12. Gladkikh, A., Feranchuk, S., Ponomareva, A., Bochalgin, N. & Mironova, L. Antibiotic resistance in *Vibrio cholerae* El Tor strains isolated during cholera complications in Siberia and the Far East of Russia. *Infect. Genet. Evol.* **78**, 104096 (2020).
13. Munita, J. M. & Arias, C. A. Mechanisms of antibiotic resistance. *Virulence mechanisms of bacterial pathogens* 481–511 (2016).
14. Weill, F.-X. et al. Genomic history of the seventh pandemic of cholera in Africa. *Science* **358**, 785–789 (2017).
15. Kumar, P. et al. Emergence of Haitian variant genotype and altered drug susceptibility in *Vibrio cholerae* O1 El Tor-associated cholera outbreaks in Solapur, India. *Int. J. Antimicrobial Agents* **55**, 105853 (2020).
16. Sengupta, T. K. et al. Interaction of *Vibrio cholerae* cells with beta-lactam antibiotics: Emergence of resistant cells at a high frequency. *Antimicrob. Agents Chemother.* **36**, 788–795 (1992).
17. Massad, E., Lundberg, S. & Yang, H. M. Modeling and simulating the evolution of resistance against antibiotics. *Int. J. Biomed. Comput.* **33**, 65–81 (1993).
18. Mushanyu, J. Mathematical modelling of community acquired antibiotic resistant infections. *Inform. Med. Unlocked* **45**, 101452 (2024).
19. Castillo-Chavez, C. & Feng, Z. To treat or not to treat: The case of tuberculosis. *J. Math. Biol.* **35**, 629–656 (1997).
20. Webb, G. F., D'Agata, E. M., Magal, P. & Ruan, S. A model of antibiotic-resistant bacterial epidemics in hospitals. *Proc. Natl. Acad. Sci.* **102**, 13343–13348 (2005).
21. Haber, M., Levin, B. R. & Kramarz, P. Antibiotic control of antibiotic resistance in hospitals: A simulation study. *BMC Infect. Dis.* **10**, 1–10 (2010).
22. Chow, K., Wang, X., Curtiss, R. III. & Castillo-Chavez, C. Evaluating the efficacy of antimicrobial cycling programmes and patient isolation on dual resistance in hospitals. *J. Biol. Dyn.* **5**, 27–43 (2011).
23. Kitaoka, M., Miyata, S. T., Unterweger, D. & Pukatzki, S. Antibiotic resistance mechanisms of *Vibrio cholerae*. *J. Med. Microbiol.* **60**, 397–407 (2011).
24. O'grady, E., Lewis, M. & Pearson, N. Global surveillance of antibiotic sensitivity of *Vibrio cholerae*. *Bull. World Health Organ.* **54**, 181 (1976).
25. Mushayabasa, S. & Bhunu, C. P. Assessing the impact of increasing antimicrobial resistance of *Vibrio cholerae* on the future trends of cholera epidemic. *International Scholarly Research Notices* **2012** (2012).
26. Safi, M. A., Melesse, D. Y. & Gumel, A. B. Dynamics analysis of a multi-strain cholera model with an imperfect vaccine. *Bull. Math. Biol.* **75**, 1104–1137 (2013).
27. Mushanyu, J., Matsebulu, L. M., Nuugulu, S. M. & Shikongo, A. Modeling the dynamics of anti-microbial resistant cholera infection with reinfection. *Franklin Open* **7**, 100111 (2024).
28. Levin, B. R. Minimizing potential resistance: A population dynamics view. *Clin. Infect. Dis.* **33**, S161–S169 (2001).
29. Blower, S., Small, P. & Hopewell, P. Control strategies for tuberculosis epidemics: New models for old problems. *Science* **273**, 497–500 (1996).
30. Mushanyu, J., Chukwu, C. W., Madubueze, C. E., Chazuka, Z. & Ogbogbo, C. P. A deterministic compartmental model for investigating the impact of escapees on the transmission dynamics of covid-19. *Healthc. Analyt.* **4**, 100275 (2023).
31. Peter, O. J., Panigoro, H. S., Abidemi, A., Ojo, M. M. & Oguntolu, F. A. Mathematical model of covid-19 pandemic with double dose vaccination. *Acta. Biotheor.* **71**, 9 (2023).
32. Abioye, A. I., Peter, O. J., Addai, E., Oguntolu, F. A. & Ayoola, T. A. Modeling the impact of control strategies on malaria and covid-19 coinfection: Insights and implications for integrated public health interventions. *Quality Quant.* **58**, 3475–3495 (2024).
33. Omede, B. I., Bolaji, B., Peter, O. J., Ibrahim, A. A. & Oguntolu, F. A. Mathematical analysis on the vertical and horizontal transmission dynamics of HIV and Zika virus co-infection. *Franklin Open* 100064 (2023).
34. Asamoah, J. K. K. et al. Backward bifurcation and sensitivity analysis for bacterial meningitis transmission dynamics with a nonlinear recovery rate. *Chaos Solit. Fract.* **140**, 110237 (2020).
35. Asamoah, J. K. K. et al. Optimal control dynamics of gonorrhoea in a structured population. *Heliyon* **9** (2023).
36. Addai, E., Torres, D. F., Abdul-Hamid, Z., Mezue, M. N. & Asamoah, J. K. K. Modelling the dynamics of online food delivery services on the spread of food-borne diseases. *Modeling Earth Systems and Environment* 1–16 (2024).
37. Adu, I. K. et al. Modelling the dynamics of ebola disease transmission with optimal control analysis. *Modeling Earth Systems and Environment* 1–27 (2024).
38. Peter, O. J., Cattani, C. & Omame, A. Modelling transmission dynamics of measles: The effect of treatment failure in complicated cases. *Modeling Earth Systems and Environment* 1–19 (2024).
39. Mushanyu, J., Nyabadza, F., Muchatibaya, G., Mafuta, P. & Nshawu, G. Assessing the potential impact of limited public health resources on the spread and control of typhoid. *J. Math. Biol.* **77**, 647–670 (2018).
40. Rahmi, E., Anggriani, N., Panigoro, H. S., Cahyono, E. & Peter, O. J. Untangling the memory and inhibitory effects on sis-epidemic model with beddington-deangelis infection rate. *Res. Control Optim.* **16**, 100458 (2024).
41. Asamoah, J. K. K. et al. Global stability and cost-effectiveness analysis of covid-19 considering the impact of the environment: Using data from ghana. *Chaos Solit. Fract.* **140**, 110103 (2020).
42. Mushanyu, J., Nyabadza, F., Muchatibaya, G. & Stewart, A. Modelling drug abuse epidemics in the presence of limited rehabilitation capacity. *Bull. Math. Biol.* **78**, 2364–2389 (2016).
43. Opatowski, L., Guillemot, D., Boëlle, P.-Y. & Temime, L. Contribution of mathematical modeling to the fight against bacterial antibiotic resistance. *Curr. Opin. Infect. Dis.* **24**, 279–287 (2011).
44. Lipsitch, M., Bergstrom, C. T. & Levin, B. R. The epidemiology of antibiotic resistance in hospitals: Paradoxes and prescriptions. *Proc. Natl. Acad. Sci.* **97**, 1938–1943 (2000).
45. Nelson, E. J., Harris, J. B., Morris, J. G., Calderwood, S. B. & Camilli, A. Cholera transmission: The host, pathogen, and bacteriophage dynamic. *Nat. Rev. Microbiol.* **7**, 693–702 (2009).
46. Van den Driessche, P. & Watmough, J. Reproduction numbers and sub-threshold endemic equilibria for compartmental models of disease transmission. *Math. Biosci.* **180**, 29–48 (2002).
47. Chitnis, N., Hyman, J. M. & Cushing, J. M. Determining important parameters in the spread of malaria through the sensitivity analysis of a mathematical model. *Bull. Math. Biol.* **70**, 1272–1296 (2008).

48. Castillo-Chavez, C. & Song, B. Dynamical models of tuberculosis and their applications. *Math. Biosci. Eng.* **1**, 361–404 (2004).
49. Codeço, C. T. Endemic and epidemic dynamics of cholera: The role of the aquatic reservoir. *BMC Infect. Dis.* **1**, 1–14 (2001).
50. Miller Neilan, R. L., Schaefer, E., Gaff, H., Fister, K. R. & Lenhart, S. Modeling optimal intervention strategies for cholera. *Bull. Math. Biol.* **72**, 2004–2018 (2010).
51. King, A. A., Ionides, E. L., Pascual, M. & Bouma, M. J. Inapparent infections and cholera dynamics. *Nature* **454**, 877–880 (2008).
52. Hartley, D. M., Morris, J. G. Jr. & Smith, D. L. Hyperinfectivity: a critical element in the ability of *V. cholerae* to cause epidemics?. *PLoS Med.* **3**, e7 (2006).
53. Metropolis, N., Rosenbluth, A. W., Rosenbluth, M. N., Teller, A. H. & Teller, E. Equation of state calculations by fast computing machines. *J. Chem. Phys.* **21**, 1087–1092 (1953).
54. Hastings, W. K. Monte Carlo sampling methods using Markov Chains and their applications. *Biometrika* **57**, 97–109 (1970).
55. Gelfand, A. E. & Smith, A. F. Sampling-based approaches to calculating marginal densities. *J. Am. Stat. Assoc.* **85**, 398–409 (1990).
56. Geman, S. & Geman, D. Stochastic relaxation, Gibbs distributions, and the Bayesian restoration of images. *IEEE Trans. Pattern Anal. Mach. Intell.* 721–741 (1984).
57. Hoffman, M. D. & Gelman, A. The No-U-Turn sampler: Adaptively setting path lengths in Hamiltonian Monte Carlo. *J. Mach. Learn. Res.* **15**, 1593–1623 (2014).
58. Caughey, D. & Wang, M. Dynamic ecological inference for time-varying population distributions based on sparse, irregular, and noisy marginal data. *Polit. Anal.* **27**, 388–396 (2019).
59. Vehtari, A., Gelman, A. & Gabry, J. Practical Bayesian model evaluation using leave-one-out cross-validation and WAIC. *Stat. Comput.* **27**, 1413–1432 (2017).
60. Carpenter, B. et al. Stan: A probabilistic programming language. *J. Stat. Softw.* **76**, 1–32 (2017).
61. Betancourt, M. & Girolami, M. Hamiltonian Monte Carlo for hierarchical models. *Current Trends Bayesian Methodol. Appl.* **79**, 2–4 (2015).
62. OCHA Haiti. Haiti cholera data (2024). Accessed: 2024-10-02.
63. McKay, M. D., Beckman, R. J. & Conover, W. J. A comparison of three methods for selecting values of input variables in the analysis of output from a computer code. *Technometrics* **21**, 239–245 (1979).
64. Spearman, C. The proof and measurement of association between two things. *Am. J. Psychol.* **15**, 72–101 (1904).

Acknowledgements

The authors acknowledge, with thanks, the support of their respective departments towards producing this manuscript.

Author contributions

J.M. conceptualized the model, J.M and F.N. carried out the model analysis, L.M. conducted data curation and numerical simulations of the model. All authors carried out the compilation of the results. All authors edited and reviewed the manuscript.

Declarations

Competing interests

The authors declare no competing interests.

Additional information

Correspondence and requests for materials should be addressed to J.M.

Reprints and permissions information is available at www.nature.com/reprints.

Publisher's note Springer Nature remains neutral with regard to jurisdictional claims in published maps and institutional affiliations.

Open Access This article is licensed under a Creative Commons Attribution-NonCommercial-NoDerivatives 4.0 International License, which permits any non-commercial use, sharing, distribution and reproduction in any medium or format, as long as you give appropriate credit to the original author(s) and the source, provide a link to the Creative Commons licence, and indicate if you modified the licensed material. You do not have permission under this licence to share adapted material derived from this article or parts of it. The images or other third party material in this article are included in the article's Creative Commons licence, unless indicated otherwise in a credit line to the material. If material is not included in the article's Creative Commons licence and your intended use is not permitted by statutory regulation or exceeds the permitted use, you will need to obtain permission directly from the copyright holder. To view a copy of this licence, visit <http://creativecommons.org/licenses/by-nc-nd/4.0/>.

© The Author(s) 2024